Journal of Medicinal Chemistry

pubs.acs.org/jmc Article

Discovery of Benzopyridone-Based Transient Receptor Potential Vanilloid 1 Agonists and Antagonists and the Structural Elucidation of Their Activity Shift

Shivaji A. Thorat,[#] Yoonji Lee,[#] Aeran Jung, Jihyae Ann, Songyeon Ahn, Jisoo Baek, Dongxu Zuo, Nayeon Do, Jin Ju Jeong, Peter M. Blumberg, Timothy E. Esch, Noe A. Turcios, Larry V. Pearce, Hee-Jin Ha, Young Dong Yoo, Sunhye Hong, Sun Choi,* and Jeewoo Lee*

Cite This: *J. Med. Chem.* 2021, 64, 370−384 Read Online

ACCESS | Metrics & More | Article Recommendations | Supporting Information

ABSTRACT: Among a series of benzopyridone-based scaffolds investigated as human transient receptor potential vanilloid 1 (TRPV1) ligands, two isomeric benzopyridone scaffolds demonstrated a consistent and distinctive functional profile in which 2-oxo-1,2-dihydroquinolin-5-yl analogues (e.g., **2**) displayed high affinity and potent antagonism, whereas 1-oxo-1,2-dihydroisoquinolin-5-yl analogues (e.g., **3**) showed full agonism with high potency. Our computational models provide insight into the agonist−antagonist boundary of the analogues suggesting that the Arg557 residue in the S4−S5 linker might be important for sensing the agonist binding and transmitting signals. These results provide structural insights into the TRPV1 and the protein−ligand interactions at a molecular level.

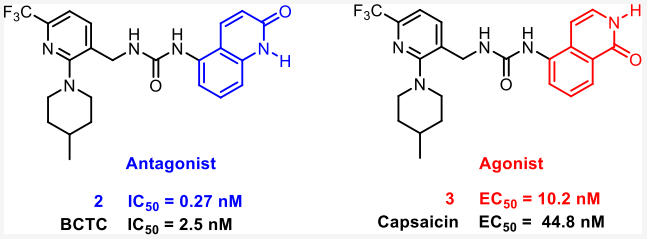

1. INTRODUCTION

Transient receptor potential vanilloid 1 (TRPV1) is a molecular integrator of nociceptive stimuli expressed in primary C-fiber sensory neurons and represents a promising therapeutic target for the treatment of neuropathic pain and a wide range of other conditions in which C-fiber sensory neurons are involved.[1,2] TRPV1 is nonselective cation channel with high Ca^{2+} permeability[3] and is activated by endogenous factors such as noxious heat, low pH, and endovanilloids as well as by natural ligands such as capsaicin and resiniferatoxin (RTX). Also, it is responsive to the state of the signaling pathways in the cells.[3−6]

TRPV1 shares many structural features with other ion channels, such as the voltage-gated potassium channel, being assembled as a tetramer.[3] The recent success of transmission electron cryomicroscopy (cryo-EM) studies of TRPV1 not only confirmed that the peripheral domain in each subunit, encompassing S1−S4 segments, is connected to the pore domains (S5 and S6) by a short linker, but also showed several structural states under different conditions: in the absence of ligand, in the presence of known agonists, that is, capsaicin or RTX, and in the presence of known antagonist, capsazepine.[7,8]

The receptor activation leads to an increase in intracellular Ca^{2+} that results in excitation of primary sensory neurons and ultimately in the central perception of harmful stimuli such as pain, itching, burning, and stinging sensations. The blocking of this activation could be obtained by antagonism as well as by desensitization upon persistent activation of agonist, suggesting that both functional activities could have considerable therapeutic utility.

The agonist causes the persistent activation of the channel resulting in high intracellular levels of calcium, ultimately leading to desensitization/defunctionalization of a variety of noxious stimuli to the peripheral ends of nerve fibers and consequent pain relief.[9] The antagonists have a therapeutic advantage over agonists in that they lack the initial excitatory effect preceding the desensitization, which represents a limiting toxicity for the systemic application of the agonists. However, their clinical development has been complicated by side effects such as hyperthermia and an increased heat perception threshold and by their nonselective antagonism, which blocks all modes of TRPV1 activation.[10−13] In consequence, both selective antagonists, which inhibit only the activators related to pain perception[12,13] and nonpungent agonists with minimal initial excitation[14] represent second generation objectives for TRPV1 clinical candidates.

The pharmacophore of TRPV1 ligands can be divided into three regions, so-called A-, B-, and C-regions, as previously designated for capsaicin and as described in our prototype

Received: June 9, 2020
Published: January 1, 2021

https://dx.doi.org/10.1021/acs.jmedchem.0c00982
J. Med. Chem. 2021, 64, 370−384

antagonist **1** (Figure 1).[15] The C-region of **1**, the 6-(trifluoromethyl)-2-(4-methylpiperidin-1-yl)pyridine group, in

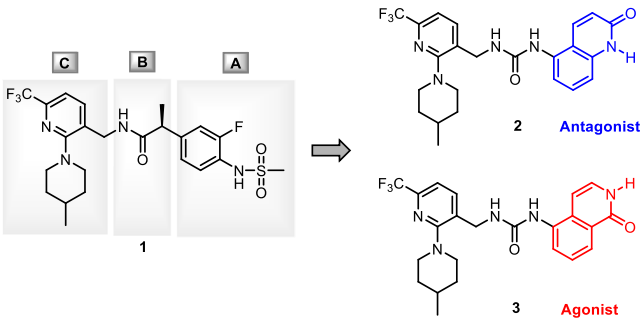

Figure 1. Discovery of benzopyridone-based TRPV1 antagonist and agonist.

the C-region library has been shown to confer high potency in our TRPV1 antagonists,[16] representing as a prototype of the C-region for the structure activity relationship (SAR) study of A- and B-regions. The urea group has been much employed as the B-region because it provides both high potency and synthetic accessibility.

In our program to discover novel potent TRPV1 ligands as drug candidates, we have investigated a series of heterocyclic A-region analogues in which the B- and C-regions were fixed with a urea and the prototype pyridine of **1**, respectively. Among the analogues studied, we demonstrated that the two isomeric benzopyridone scaffolds exhibited distinctive functional profiles in which 2-oxo-1,2-dihydroquinolin-5-yl (e.g., **2**) and 1-oxo-1,2-dihydroisoquinolin-5-yl (e.g., **3**) A-region derivatives provided potent antagonism and agonism, respectively, with human TRPV1 (*h*TRPV1), and their functional activities were maintained over the range of C-regions investigated.

In this study, we describe the SAR of a series of benzopyridone A-region analogues to examine their functional activities. With the selected benzopyridone A-regions, we further investigated the SAR of the C-region to explore the maintenance of functional activity as well as to improve the potency. To confirm the in vitro mechanism of action of the optimized agonist and antagonist, we evaluated their effects on body temperature in the animal as an in vivo study. Finally, in order to elucidate the structural basis for the activity shift of the two isomeric ligands, we established our revised TRPV1 homology model based on the cryogenic electron microscopy (cryo-EM) structure of rat TRPV1 (*r*TRPV1) and performed molecular modeling studies to gain structural insights into the activities of the ligands by identifying the key binding interactions critical for their agonism and antagonism.

2. RESULTS AND DISCUSSION

2.1. Chemistry. The final urea compounds were generally synthesized by the coupling between the carbamate of the benzopyridone A-region and the amine of the pyridine/pyrazole C-region, respectively. The syntheses of the benzopyridone A-region are represented in Schemes 1−3 and the pyridine and pyrazole C-region amines were prepared by the previous reports,[16] respectively.

For the syntheses of 2-oxo-1,2-dihydroquinolin-5 (or 8)-yl A-region analogues (Scheme 1), the nitration of 2-chloroquinoline afforded a mixture of 5-nitro (**5**) and 8-nitro (**6**) isomers in a 1:2 ratio. The isomers were hydrolyzed under acidic conditions into the corresponding 2-pyridones, respectively, in which 5-nitro pyridone was further N-methylated. The nitro groups of benzopyridone intermediates were hydrogenated to the corresponding amines (**7**, **8**, **12**), which were converted to the corresponding phenyl carbamates (**9**, **10**, **13**), respectively. Finally, the coupling of the carbamates with the pyridine C-region amine[15] provided 2-oxo-1,2-dihydroquinolin-5-yl (**2**), 1-methyl-2-oxo-1,2-dihydroquinolin-5-yl (**11**), and 2-oxo-1,2-dihydroquinolin-8-yl (**14**) ureas, respectively.

For the synthesis of 1-oxo-1,2-dihydroisoquinolin-5-yl A-region analogues (Scheme 2), 1-chloroisoquinoline was hydrolyzed to the corresponding 2-pyridone and then nitrated to give 5-nitro isoquinolin-1-one **16**. The nitro reduction or N-methylation followed by reduction of **16** afforded **17** and **18**, respectively, which were converted to the final ureas (**3**, **19**) by employing the same route as discussed above. For the synthesis of the 1-oxo-1,2-dihydroisoquinolin-8-yl A-region analogue (Scheme 2), isoquinoline was brominated and then selectively nitrated to give 8-nitro isoquinoline **21**. The N-oxidation of **21** followed by rearrangement with acetic anhydride[17] provided the corresponding pyridone, which was reduced to amine **22** and then converted to the final compound (**23**).

For the syntheses of 2-oxo-1,2-dihydroquinolin-6-yl and 1-oxo-1,2-dihydroisoquinolin-7-yl A-region analogues (Scheme

Scheme 1. General Procedures of 2-Oxo-1,2-dihydroquinolin-5 (or 8)-yl A-Region Analogues[a]

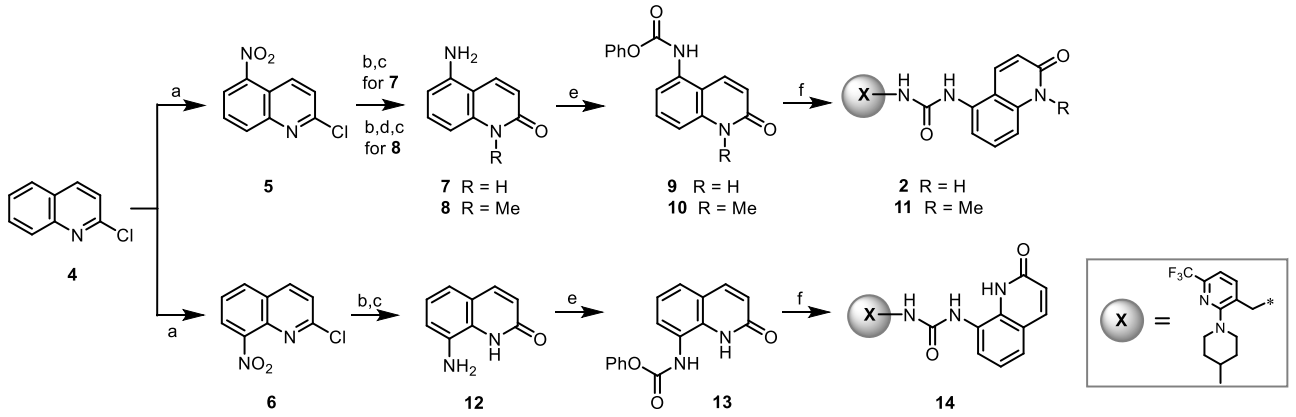

[a]Reagents and conditions: (a) KNO_3, H_2SO_4 (**5** (20%), **6** (40%)); (b) 5 N HCl, THF; (c) 10% Pd/C, EtOH; (d) NaH, MeI; (e) PhOCOCl, pyridine, THF−DMF (1:1); and (f) X−NH_2, NEt_3, DMF.

https://dx.doi.org/10.1021/acs.jmedchem.0c00982
J. Med. Chem. 2021, 64, 370−384

Scheme 2. General Procedures of 1-Oxo-1,2-dihydroisoquinolin A-Region Analogues[a]

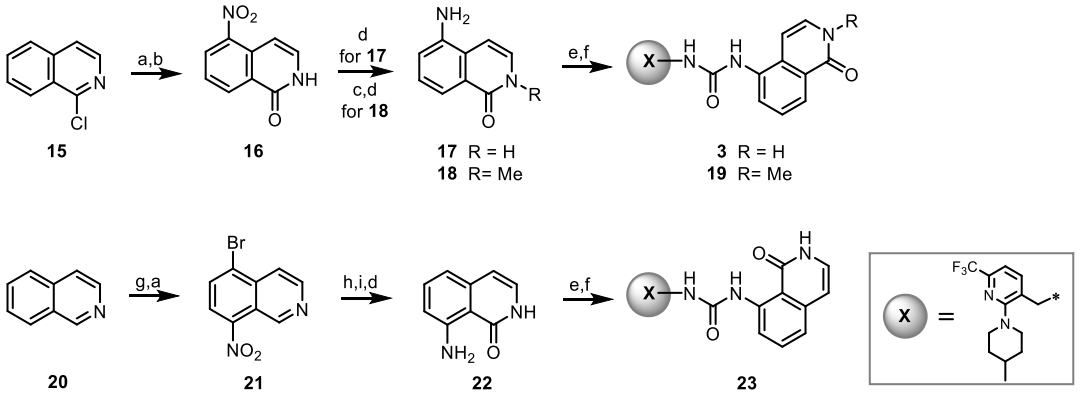

[a]Reagents and conditions: (a) KNO_3, H_2SO_4; (b) 5 N HCl, THF; (c) NaH, MeI, THF; (d) 10% Pd/C, H_2, MeOH; (e) PhOCOCl, pyridine, ACN−THF (1:1); (f) X−NH_2, NEt_3, DMF; (g) NBS, H_2SO_4; (h) H_2O_2, AcOH; and (i) Ac_2O, 10% K_2CO_3.

Scheme 3. General Procedures of 2-Oxo-1,2-dihydroquinolin A-Region Analogues[a]

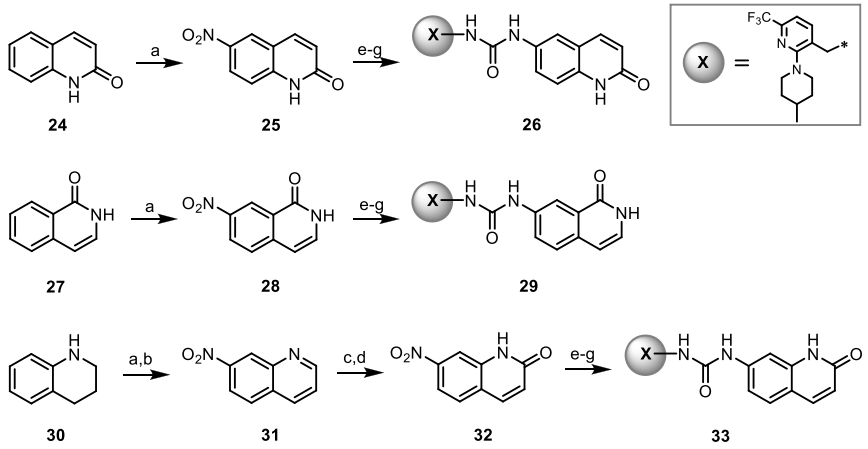

[a]Reagents and conditions: (a)KNO_3, H_2SO_4; (b) DDQ, DCM; (c) mCPBA, DCM; (d) TFAA, DMF; (e) 10% Pd/C, H_2, MeOH; (f) PhOCOCl, pyridine, THF; and (g) X−NH_2, NEt_3, DMF.

Scheme 4. General Procedures of 5-aminoisoquinolinone A-Region Analogue[a]

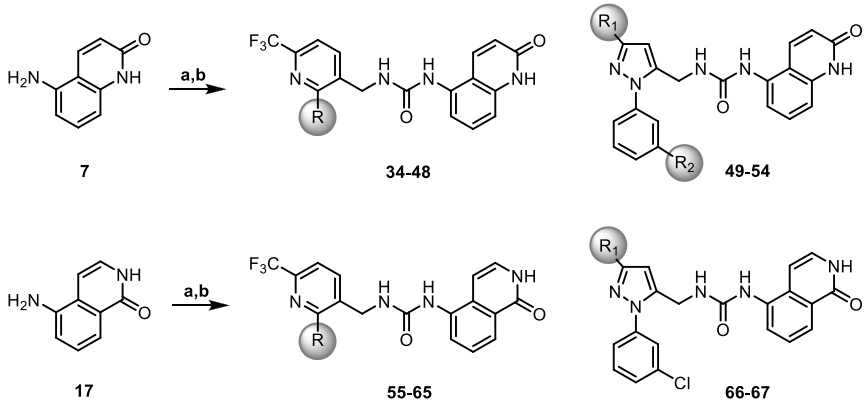

[a]Reagents and conditions: (a) PhOCOCl, pyridine, THF; (b) C-region amine, NEt_3, DMF.

3), quinolin-2-one and isoquinolin-2-one were selectively nitrated, respectively, and then converted to the final ureas (**26**, **29**) by following the same routes as discussed above. For the synthesis of the 2-oxo-1,2-dihydroquinolin-7-yl A-region analogue, 7-nitroquinoline **31** was prepared from 1,2,3,4-tetrahydroquinoline by selective nitration followed by ring oxidation. The N-oxidation of **31** followed by rearrangement provided the corresponding pyridone **32**, which was converted to the final compound (**33**).

For the syntheses of the C-region analogues of **2** and **3** (Scheme 4), 5-aminoquinolin-2-one **7** and 5-aminoisoquinolin-1-one **17** were converted to the corresponding carbamates, respectively, which were reacted with various pyridine and pyrazole C-region amines previously reported[16] to provide the

https://dx.doi.org/10.1021/acs.jmedchem.0c00982
J. Med. Chem. 2021, 64, 370−384

final 2-oxo-1,2-dihydroquinolin-5-yl (**34**−**54**) and 1-oxo-1,2-dihydroisoquinolin-5-yl (**55**−**67**) derivatives.

2.2. Structure Activity Relationship. The binding affinities and functional potencies of TRPV1 ligands with the benzopyridone A-region in Table 1 were assessed in vitro by a

Table 1. SAR of Benzopyridone A-Region on *h*TRPV1[a]

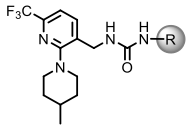

	R	Binding Affinity K_i (nM)	Agonism EC_{50} (nM)	Antagonism K_i (nM)
1		2.95	NE	1.26
2		0.72	NE	3.94
11		0.57	NE	2.59
3		35.3	9.59	NE
19		589	2%[b]	82%[c]
14		492	NE	441
23		239	NE	70%[c]
26		39.9	40%[b]	37%[c]
29		215	NE	90.7
33		2.95	NE	0.83

[a]NE: no effect, WE: weak effect; the values are the mean of at least three experiments. NE, results of at least two experiments. [b]Only fractional calcium uptake compared to 1 μM capsaicin. [c]Only fractional antagonism to 30 nM capsaicin.

binding competition assay with [^{3}H]RTX and by a functional $^{45}Ca^{2+}$ uptake assay using *h*TRPV1 heterologously expressed in Chinese hamster ovary (CHO) cells, as previously described.[18] For the agonism assay, a saturating concentration of capsaicin (1 μM) was used to define maximal response. For the antagonism assay, the dose-dependent inhibition of the capsaicin (30 nM)-stimulated calcium uptake was measured. The K_i values for antagonism take into account the competition between capsaicin and the antagonist.[19]

To evaluate the antagonistic potency of the compounds in Tables 2 and 3 for *h*TRPV1, assays were conducted using a fluorometric imaging plate reader (FLIPR) with *h*TRPV1

Table 2. SAR of the Pyridine C-Region in 2 on *h*TRPV1[a]a

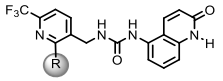

	R	IC_{50} (nM)		R	IC_{50} (nM)
BCTC		2.5			
2		0.27	**41**		2.60
34		0.75	**42**		1.49
35		1.59	**43**		2.18
36		0.94	**44**		1.20
37		5.21	**45**		2.15
38		4.00	**46**		1.44
39		2.72	**47**		1.35
40		3.19	**48**		1.93

[a]The values are the mean of at least three experiments.

Table 3. SAR of the Pyrazole C-Region in 2 on *h*TRPV1[a]

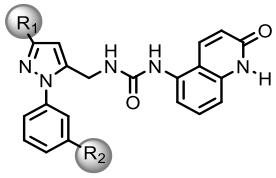

	R_1	R_2	IC_{50} (nM)
49	CF_3	Cl	1.71
50		F	1.28
51		CH_3	0.64
52		$CHMe_2$	0.88
53	t-Bu	Cl	4.41
54		F	6.17

[a]The values are the mean of at least three experiments.

heterologously expressed in recombinant human embryonic kidney (HEK) cells.[15] The antagonistic activity was measured by inhibition of TRPV1 activation by capsaicin (10 nM) and was compared to that of the prototype antagonist, BCTC ($K_{i(CAP)}$ = 2.5 nM). To measure the agonistic potency of the compounds in Table 4 for *h*TRPV1, a functional $^{45}Ca^{2+}$ uptake assay as

https://dx.doi.org/10.1021/acs.jmedchem.0c00982
J. Med. Chem. 2021, 64, 370−384

described in Table 1 was used and the activities were compared to that of the prototype agonist, capsaicin (EC_{50} = 44.8 nM).

Table 4. SAR of the C-Region in 3 on *h*TRPV1[a]

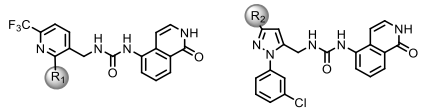

	R_1	EC_{50} (nM)[b]		R_1	EC_{50} (nM)[b]
Capsaicin		44.8			
3		10.2	**60**		78.7
55		13.2	**61**		63.2
56		5.81	**62**		15.5
57		258	**63**		78.6
58		2.79	**64**		69.3
59		160	**65**		3.07
	R_2			R_2	
66	CF_3	41.4	**67**	t-Bu	9.59

[a]The values are the mean of at least three experiments. [b]All showed no antagonistic activity in the assay.

First, we investigated the structural and positional benzopyridone isomers in the A-region analogues with the B- and C-regions fixed with a urea and prototype pyridine. The 2-oxo-1,2-dihydroquinolin-5-yl A-region analogue (**2**) showed high affinity with a K_i = 0.72 nM and potent antagonism with a $K_{i(ant)}$ = 3.94 nM, which was 4-fold higher in binding affinity and 3-fold weaker in antagonistic potency compared to reference **1**, respectively. Its *N*-methyl analogue (**11**) exhibited similar binding affinity and antagonism compared to **2**, suggesting that N−H of pyridone was not involved in hydrogen bonding with the receptor for activity. On the contrary, the 1-oxo-1,2-dihydroisoquinolin-5-yl A-region analogue (**3**), a reverse amide surrogate of **2**, proved to be a full and potent agonist with an EC_{50} = 9.6 nM. However, its N-methylation, providing **19**, led to much reduction in binding affinity and caused the shift of functional activity toward antagonism, revealing that the N−H group of the pyridone in **3** was critical for interacting with the receptor for agonism. Next, we explored the positional isomers of **2** and **3**. 2-Oxo-1,2-dihydroquinolin-8-yl (**14**) and 1-oxo-1,2-dihydroisoquinolin-8-yl (**23**) analogues showed very weak binding affinity and antagonism, indicating that their ring amides directed to the urea probably caused unfavorable interaction with the receptor. Other positional analogues, **26**, **29**, and **33**, were also explored as positional isomers. Whereas the 2-oxo-1,2-dihydroquinolin-6-yl (**26**) and 1-oxo-1,2-dihydroisoquinolin-7-yl (**29**) analogues were a partial agonist and a weak antagonist, respectively, the 2-oxo-1,2-dihydroquinolin-7-yl analogue (**33**) was found to be very potent antagonist with a $K_{i(ant)}$ = 0.83 nM.

The findings of potent antagonist **2** and agonist **3** prompted us to explore the SAR of their C-region for further optimization. First, the 2-position in the pyridine C-region of **2** was modified with representative substituents selected from our previous study.[15] Their antagonistic activities were measured by the FLIPR assay and their values are represented in Table 2. In this assay, **2** showed excellent antagonism with an IC_{50} = 0.27 nM, which was *ca.* 10-fold more potent than BCTC. The pyridine C-region analogues, including 2-alkylamino (**34**−**37**), 2-alkyloxy (**38**−**44**), 2-alkylthio (**45**), and alkyl/aryl (**46**−**48**) groups, all exhibited potent antagonism within the range of IC_{50} = 0.75−5.21 nM. In addition, the selected pyrazole C-region[16] analogues of **2** were also examined as shown in Table 3. They also displayed potent antagonism with a range of IC_{50} = 0.64−6.17 nM, similar to that found with the pyridine C-region. The result indicated that the 2-oxo-1,2-dihydroquinolin-5-yl A-region proved a robust antagonistic scaffold providing potent antagonism tolerant of significant variation in the C-region.

Next, we explored the C-region analogues of agonist **3**. In the calcium influx assay, **3** was found to be *ca.* 4.5-fold more potent than capsaicin. As conducted in the SAR of antagonist **2**, a series of 2-substituted pyridine and pyrazole C-region analogues of **3** (**55**−**67**) were investigated and all were found to be agonists. Among them, compounds **56**, **58**, and **65** displayed more potent agonism than **3** with values of IC_{50} = 5.81, 2.79, and 3.07 nM, which were 8−16 fold more potent than that of capsaicin. The results confirmed that 1-oxo-1,2-dihydroisoquinolin-5-yl A-region proved to be a promising agonistic scaffold showing potent agonism regardless of the C-region.

2.3. In vivo Study. It should be noted that TRPV1 modulates not only pain perception, but also other sensory modalities such as thermal control and heat perception.[1] In

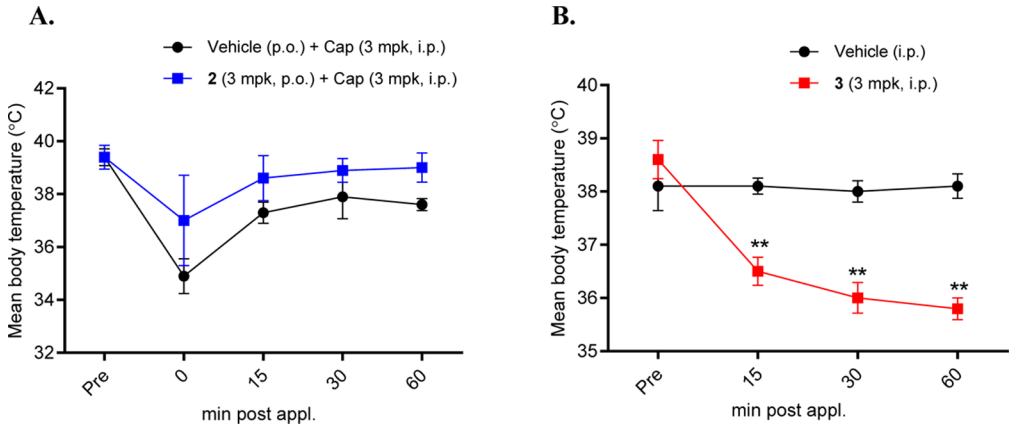

Figure 2. Body temperature study of **2** and **3**.

https://dx.doi.org/10.1021/acs.jmedchem.0c00982
J. Med. Chem. 2021, 64, 370−384

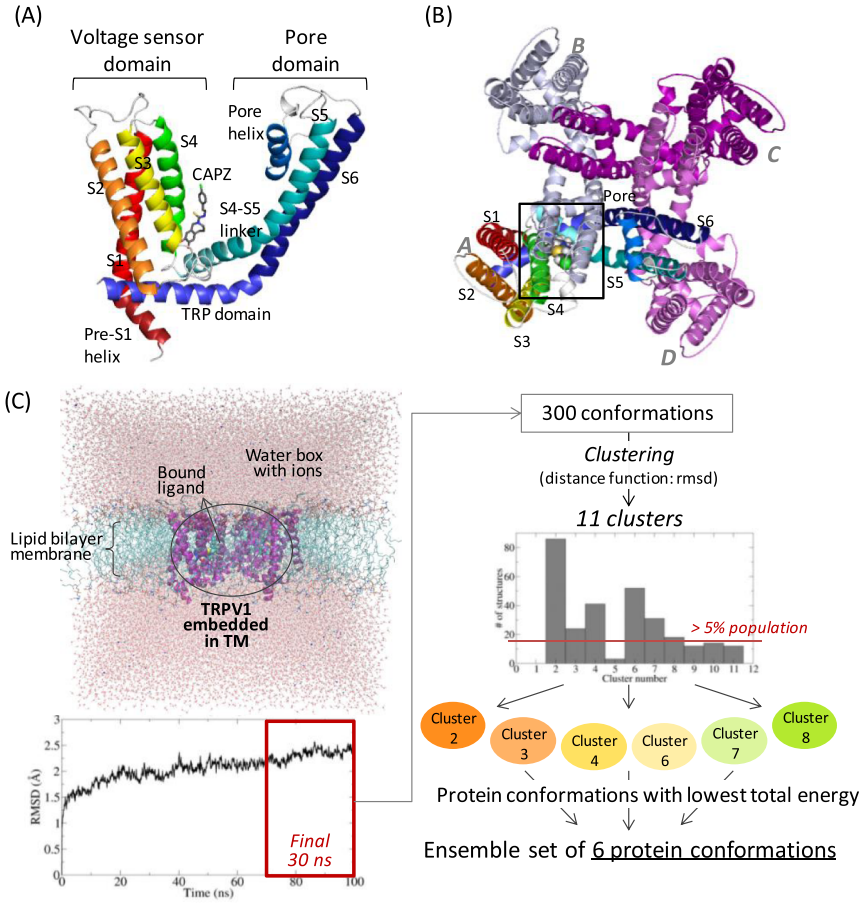

Figure 3. Homology model of *h*TRPV1. (A) Monomeric model. Six transmembrane helices (S1−S6) including pre-S1 helix, S4−S5 linkers, pore-helix, and TRP domain are marked. The bound ligand, CAPZ, is depicted in sticks. (B) Tetrameric model. The four chains are marked with A−D. Note that the ligand-binding site is composed of S3, S4, and the S4−S5 linkers of one monomer, and the S5 and S6 of the adjacent monomer (black box). (C) Generation of the MD-based multiple receptor conformations. Input system for MD simulations was represented. The graph below is for the root mean squared deviation (rmsd) plot of the 100 ns production run. From the final 30 ns MD-simulated trajectories, 300 conformations were sampled and clustered based on their rmsd values. Among the 11 clusters, highly populated clusters were chosen, and the protein conformation with lowest total energy in each cluster is selected.

particular, the regulation of body temperature is a predominant function of TRPV1 in which agonism causes a decrease in body temperature (hypothermia) and antagonism elicits an increase in body temperature (hyperthermia).

In order to confirm the antagonistic activities of **2** in vivo, we performed a capsaicin-induced hypothermia test in mice (Figure 2A).[14] Consistent with its in vitro mechanism of action, antagonist **2** after oral administration (3 mg/kg) blocked *ca.* 50% of the hypothermia induced by intraperitoneal (ip) injection of capsaicin (3 mg/kg). In addition, we measured the effect on body temperature of agonist **3** in mice (Figure 2B). The administration of **3** by ip injection (3 mg/kg) caused a drop in body temperature over −2 °C for 30−60 min, indicating that **3** proved to be a full agonist consistent with its in vitro mechanism.

2.4. Molecular Modeling Studies. Recently, the single-particle cryo-EM structures of *r*TRPV1 were released.[7,8] Although the resolution is not quite high enough for drug discovery purposes and some important side chains are not fully resolved, the structures showed homotetrameric functional states with the typical ligands bound to the intracellular site, the so-called vanilloid pocket, which is formed by two adjacent chains.[8] Using these structures as templates, the tetrameric homology model of the *h*TRPV1 transmembrane domain was constructed. The model was further refined by molecular dynamics (MD) simulations to obtain a more reliable structure. The ensemble docking study of TRPV1 ligands was carried out with the multiple conformation structures, representing the flexibility of the protein. Using our homology models and docking method, which were confirmed to be reliable by screening the known actives from decoy compounds, the binding modes of the representative benzopyridone-based agonists and antagonists were investigated.

2.5. Homology Modeling. In order to investigate the structural basis of the pharmacological activity shift of the analogues, we conducted computational studies. Although several cryo-EM structures of *r*TRPV1 were available,[8] the side chains that are essential for ligand binding interactions are not fully resolved, so that these structures may not be directly utilized for docking studies. Therefore, homology models of *h*TRPV1 were constructed by using these cryo-EM structures bound to an agonist, RTX (PDB id: 5IRX), and an antagonist, CAPZ (PDB id: 5IS0) as templates (Figure 3A). The quality of the initial monomer model was evaluated with a Ramachandran plot[20] and ERRAT scores[21] (Figure S1A), indicating that the backbone conformations and nonbonded atomic interactions are well modeled within the acceptable range. Then, the tetramer model was built by aligning each monomer model to

https://dx.doi.org/10.1021/acs.jmedchem.0c00982
J. Med. Chem. 2021, 64, 370−384

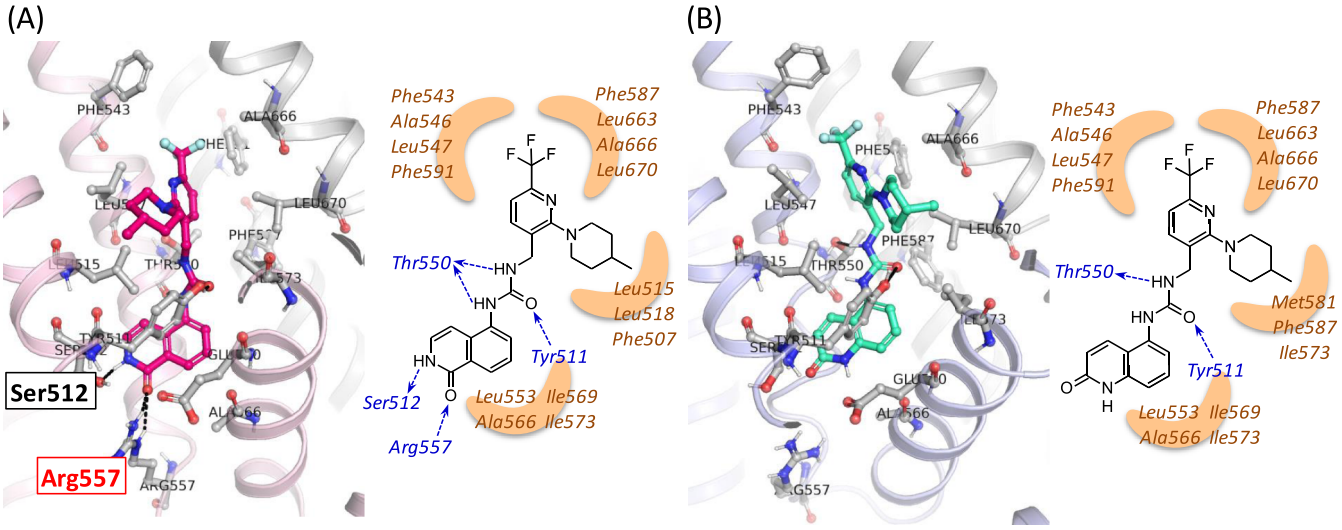

Figure 4. Binding modes of (A) the agonist **3** and (B) the antagonist **2** represented in ball-and-sticks with the carbon atoms in magenta and green-blue, respectively. The interacting residues are depicted in sticks with their carbon atoms in gray, and the hydrogen bonds are marked in black-dashed lines. The secondary structure of the *h*TRPV1 model is displayed in ribbon. The nonpolar hydrogen atoms are undisplayed for visual convenience.

the tetrameric template structure (Figure 3B), and further refined by energy-minimization and MD simulations. Because the sequence identity between *h*TRPV1 and *r*TRPV1 is almost ~93%, their overall backbone geometries can be considered to be remarkably similar. Therefore, we applied harmonic restraints to the backbone atoms to maintain the overall conformations from the experimentally determined structures. Note that the purpose of this homology modeling process was to accurately model the side chains and also to consider the dynamic aspects of the receptor's binding sites.

Because the ligand binding to a target protein is closely related to the dynamic motions of the protein, considering a protein's local flexibility or multiple conformations is crucial to increase the accuracy in modeling studies.[22] By using the MD simulations, we obtained a diverse subset of the receptor conformation structures to cover various binding site geometries. The resulting MD-derived multiple conformations were clustered based on their backbone's rmsd values, and the representative conformations (i.e., highly populated and low-energy state ones) were selected for ensemble docking studies (Figure 3C). The reliability of the models was evaluated by prescreening known active compounds (142 known TRPV1 antagonists with K_i < 1 nM in the ChEMBL database[23]) from decoy compounds (3517 drug-like molecules, which have molecular weights of 250−600 in the NCI drug database[24]). The model performed quite well for screening the known actives with the area under the receiver operating characteristic curve of 0.87 (Figure S2B).

2.6. Binding Mode Comparison of Agonists and Antagonists. For the selected representative analogues, ensemble docking studies were performed by utilizing the selected conformational ensembles of the *h*TRPV1 models. As shown in Figure 4, the agonist and antagonist showed similar binding modes with (i) the A-region, which occupies the deep bottom of the vanilloid pocket, forming hydrophobic interactions with Tyr511, Leu553, Ala566, Ile569, and Ile573, (ii) the B-region with the urea linker maintaining the key hydrogen bonds to Tyr511 and Thr550, and (iii) the C-region aromatic group, which forms additional hydrophobic interactions with the upper part residues (Phe543, Ala546, Leu547, Phe591, Ala666, and Leu670). The most significant differences between the binding modes of the agonists and antagonists were observed in the polar interaction at the bottom pocket. In the case of **3** with agonistic activity, the pyridone ring's carbonyl and NH groups showed hydrogen bonds with Arg557 and Ser512, respectively (Figure 4A). However, the reverse amide surrogate **2** cannot maintain the hydrogen bond with the residues at the bottom pocket, leading to loss of the agonistic activity (Figure 4B).

This tendency is also confirmed by other analogues with the same scaffold. For example, **56** and **58** (agonists, Figure 5A) with the A-region of **3** showed H-bonding interactions with Arg557, while **35** and **37** (antagonists, Figure 5B) with the A-

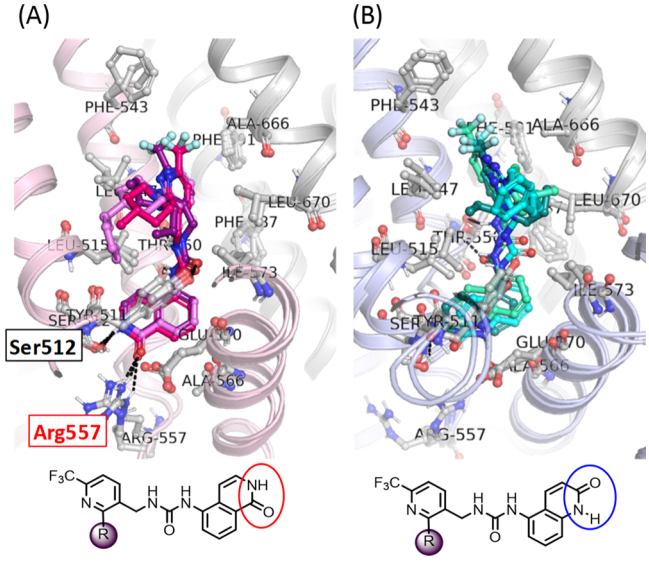

Figure 5. Overlaid binding modes of (A) the agonists **3** (magenta), **56** (light-pink), and **61** (purple) and (B) the antagonists **2** (green-blue), **35** (teal), and **37** (cyan). The interacting residues are depicted in sticks with their carbon atoms in gray, and the hydrogen bonds are marked in black-dashed lines. The secondary structure of the *h*TRPV1 model is displayed in ribbon. The nonpolar hydrogen atoms are undisplayed for visual convenience.

https://dx.doi.org/10.1021/acs.jmedchem.0c00982
J. Med. Chem. 2021, 64, 370−384

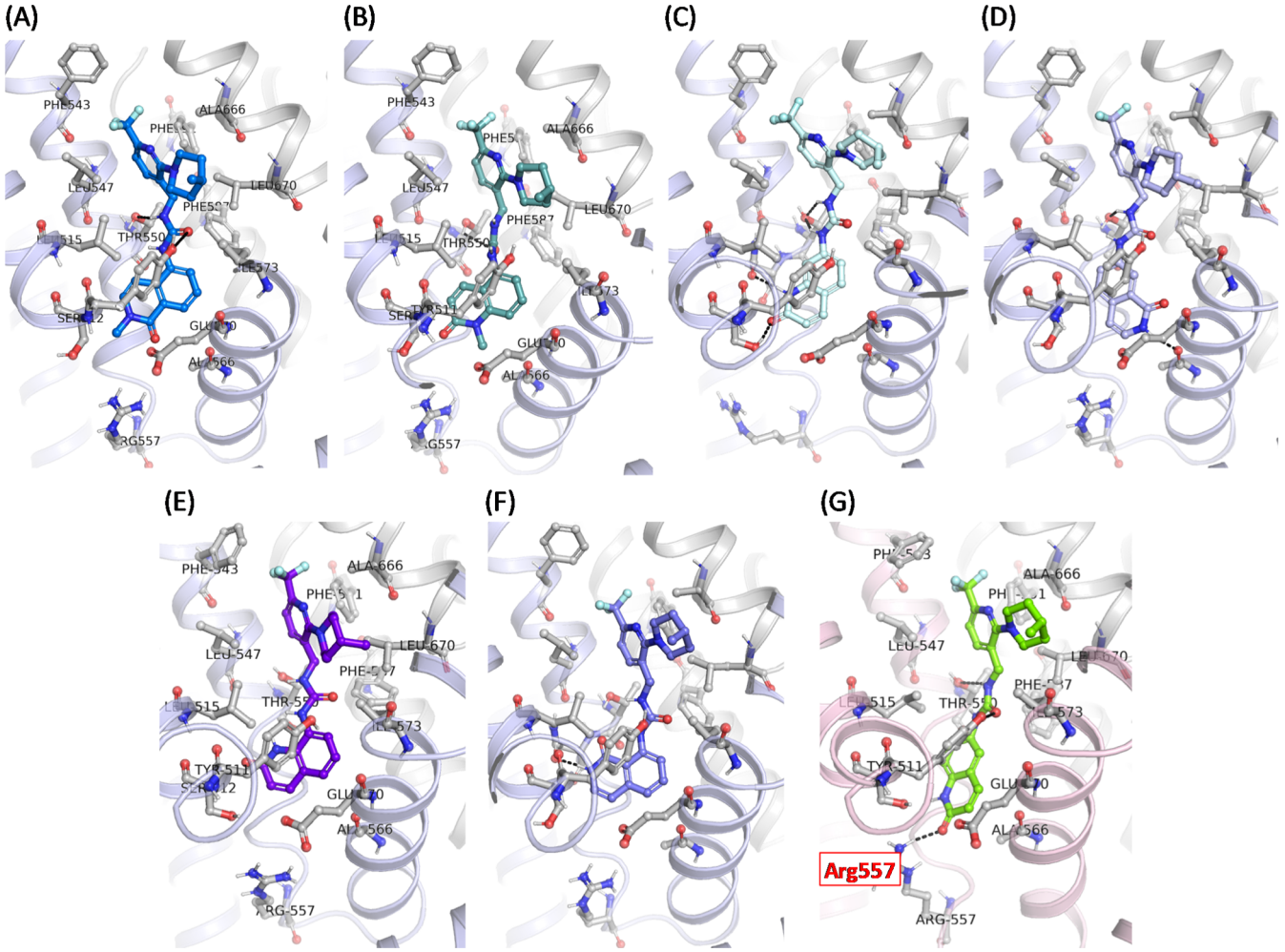

Figure 6. Binding modes of the analogues represented in ball-and-sticks with the carbon atoms in (A) sky-blue (**19**), (B) light-teal (**11**), (C) pale-cyan (**33**), (D) light-blue (**29**), (E) purple (**14**), (F) slate (**23**), and (G) green (**26**). The interacting residues are depicted in sticks with their carbon atoms in gray, and the hydrogen bonds are marked in black-dashed lines. The secondary structure of the *h*TRPV1 model is displayed in ribbon. The nonpolar hydrogen atoms are undisplayed for visual convenience.

region of **2** did not. In this scaffold, the R groups, the southern part of the C-region, can definitely contribute the hydrophobic interactions but face toward the solvent-exposed site so that the wide range of substituted groups did not alter the scaffold's pharmacological profiles (Tables 2 *vs* 4).

In addition, the compound **19**, which is the *N*-methyl analogue of **3**, cannot maintain the hydrogen bond with the residues at the bottom pocket (Figure 6A), leading to loss of agonism as well as binding affinity. It seems that, because of the spatial limitation, the additional methyl group slightly alters the binding geometry resulting in the loss of key H-bonding to the bottom residues. In the case of other antagonists **11**, **14**, **23**, **29**, and **33**, the best binding modes also did not maintain H-bonding interaction with Arg557 although they can sometimes make H-bonding with Ser512 or Ala566 at the bottom (Figure 6B−F).

The strong polar interaction with Arg557 appears to be crucial for the analogues' agonistic activities, and the proper positioning of the pyridone ring's carbonyl group makes this key interaction possible. Gao et al. also reported that Arg557 is essential for agonist binding because the agonist RTX binds to TRPV1 and coordinates the interaction between Arg557 and Glu570, consequently pulling the S4−S5 linkers away from the central axis to facilitate the opening of the lower gate.[8] Interestingly, **26**, which showed partial agonistic activity, also maintains the H-bonding with Arg557 with different binding geometry (Figure 6G).

3. CONCLUSIONS

We investigated a series of benzopyridone-based scaffolds as *h*TRPV1 ligands. Of those, the two isomeric benzopyridones, **2** and **3**, demonstrated distinctive functional profiles in which, whereas the *N*-(2-oxo-1-dihydroquinoline-5-yl) scaffold (**2**) displayed high affinity and potent antagonism, the *N*-(1-oxo-1,2-dihydroisoquinolin-5-yl) scaffold (**3**) showed full agonism with high potency. The SAR of the two scaffolds indicated that (1) the functional activities of the two scaffolds have been maintained regardless of the C-region and (2) the hydrogen bonding between pyridone of **3** and the receptor was critical for agonism. The body temperature study in mice indicated that antagonist **2** inhibited capsaicin-induced hypothermia and agonist **3** showed hypothermia in mice, consistent with the in vitro mechanism of action. Computational studies showed that the H-bonding interactions of our agonists with Arg557 in the S4−S5 linker, along with the induced-fit effect, appear to be important for sensing the agonist binding and transmitting signals. These results provide a more precise understanding of

https://dx.doi.org/10.1021/acs.jmedchem.0c00982
J. Med. Chem. 2021, 64, 370−384

the compounds' actions at the atomic level and the rationale for designing compounds with specific pharmacological profiles.

4. EXPERIMENTAL SECTION

4.1. General. All chemical reagents and solvents were commercially available. Melting points were determined on a melting point Buchi B-540 apparatus and are uncorrected. Silica gel column chromatography was performed on a silica gel 60, 230−400 mesh, Merck. ^{1}H and ^{13}C NMR spectra were recorded on a JEOL JNM-LA 300 at 300 MHz and JEOL JNM-ECZ 400S at 400 MHz. Chemical shifts are reported in ppm units with Me_4Si as a reference standard. Mass spectra were recorded on an Agilent, Q-TOF 6530 LC−MS instrument. All final compounds were purified up to more 95% purity, as determined by high-performance liquid chromatography (HPLC). HPLC was performed on an Agilent 1120 Compact LC (G4288A) instrument using an Agilent TC-C18 column (4.6 mm × 250 mm, 5 μm).

4.2. General Procedure for Nitration (Procedure A). To a mixture of quinoline or qunolinone (1.0 mmol) in H_2SO_4 was added potassium nitrate (0.99 mmol) at 0 °C. The reaction mixture was allowed to warm to room temperature and stirred for 3 h. After completion, the reaction mixture was poured onto ice, neutralized with $NaHCO_3$, and extracted with EtOAc several times. The combined organic layer was washed with brine, dried over $MgSO_4$, filtered, and concentrated in vacuo. The residue was purified by silica gel column chromatography to afford the desired product.

4.3. General Procedure for Bromination (Procedure B). To a solution of isoquinoline (1.0 mmol) in concentrated H_2SO_4 (1.29 mL/mmol) was added *N*-bromosuccinimide (1.2 mmol) by portions at −10 °C. The reaction mixture was allowed to warm to room temperature and stirred for 24 h. Then, the reaction mixture was poured onto ice water and neutralized with NaOH. The water was extracted with EtOAc, dried over $MgSO_4$, and filtered and concentrated in vacuo. The residue was purified by silica gel column chromatography to afford the desired product.

4.4. General Procedure for Aromatization (Procedure C). To a solution of **30** (1.0 mmol) in CH_2Cl_2 (1.2 mL/mmol) was added 2,3-dichloro-5,6-dicyano-1,4-benzoquinone (2.0 mmol) by portions at 0 °C. The reaction mixture was allowed to warm to room temperature and stirred for 4 h. The precipitate was filtered off and washed with CH_2Cl_2. The combined filtrate was dried over $MgSO_4$, filtered, and concentrated in vacuo. The residue was purified by column chromatography on silica gel to afford the desired product.

4.5. General Procedure for Quinolinone Synthesis (Procedure D). *4.5.1. Method A.* To a solution of the appropriate chloroquinoline (1.0 mmol) in tetrahydrofuran (THF) was added 5 N HCl and refluxed for 15 h. After completion, the reaction mixture was cooled to room temperature and diluted with water and extracted with EtOAc several times. The combined organic layer was dried over $MgSO_4$, filtered, and concentrated in vacuo. The residue was purified by silica gel column chromatography to afford the desired product.

4.5.2. Method B. To a stirred solution of appropriate bromoisoquinoline (1.0 mmol) in acetic acid was slowly added 30% hydrogen peroxide (10 mmol) and refluxed for 3 h. The mixture was cooled to room temperature and the reaction mixture was extracted with EtOAc and water. The organic phase was dried over $MgSO_4$, filtered, and concentrated in vacuo to provide bromoisoquinoline N-oxide, which was used in the next step without further purification. The crude bromoisoquinoline *N*-oxide (1.0 mmol) was suspended in acetic anhydride (2 mL/mmol) and refluxed for 3 h. After cooling, the solvent was removed under reduced pressure, the residue was dissolved in 10% potassium carbonate solution (3 mL/mmol), and stirred at room temperature for 1 h. The cold suspension was adjusted to pH = 6 using 5% citric acid solution and the crystals were filtered and concentrated. The obtained residue was triturated with ether to afford the desired product.

4.5.3. Method C. To a solution of appropriate bromoisoquinoline (1.0 mmol) in CH_2Cl_2 (9 mL/mmol) was added 3-chloroperoxybenzoic acid (1.4 mmol) at 0 °C. The mixture was stirred at room temperature for 18 h. The reaction was diluted with CH_2Cl_2 and washed with brine. The organic phase was dried over $MgSO_4$, filtered, and concentrated in vacuo to provide bromoisoquinoline *N*-oxide, which was used in the next step without further purification. A suspension of bromoisoquinoline *N*-oxide (1.0 mmol) in Dimethylformamide (DMF) (1 mL/mmol) was treated with trifluoroacetic anhydride (10 mmol) at 0 °C. The clear solution was stirred at room temperature overnight then evaporated in vacuo. The residue was diluted with aqueous $NaHCO_3$ solution and extracted with EtOAc several times. The combined organic extracts were washed with brine, dried over $MgSO_4$, and evaporated. The residue was purified by column chromatography on silica gel to afford the desired product.

4.6. General Procedure for N-Methylation (Procedure E). To a solution of 5-nitroisoquinolin-1(2*H*)-one (1.0 mmol) in DMF, sodium hydride (60% suspension oil, 1.5 mmol) was added at 0 °C and stirred for 30 min. Methyl iodide (1.3 mmol) was added and the mixture was stirred for 5 h. The reaction mixture was quenched by dropwise addition of water at 0 °C and extracted with EtOAc, washed with brine several times, dried over $MgSO_4$, and concentrated in vacuo. The residue was purified by silica gel column chromatography to afford the desired compound.

4.7. General Procedure for Catalytic Hydrogenation (Procedure F). Palladium on charcoal (10% w/w) was added to a solution of appropriate nitroquinolinone (1.0 mmol) in EtOAc or MeOH and stirred under a balloon of hydrogen for 18 h. The reaction mixture was filtered through Celite pad washing with EtOAc. The filtrate was concentrated under reduced pressure and purified by column chromatography to afford the desired compound.

4.8. General Procedure for Carbamation (Procedure G). To a solution of the appropriate amine (1.0 mmol) in THF was added pyridine (1.1 mmol) and phenyl chloroformate (1.0 mmol) at 0 °C and stirred at room temperature for 2 h. The reaction mixture was quenched with water and extracted with EtOAc several times. The combined organic layer was washed with brine, dried over $MgSO_4$, filtered, and concentrated in vacuo. The residue was purified by silica gel column chromatography to afford the desired product.

4.9. General Procedure for Urea Coupling (Procedure H). To a solution of the appropriate carbamate (1.0 mmol) in DMF was added amine (2.0 mmol) and triethylamine (1.0 mmol) and stirred at 50 °C for 15 h. After completion, the reaction mixture was cooled to room temperature, diluted with water, and extracted with EtOAc several times. The combined organic layer was washed with brine, dried over $MgSO_4$, filtered, and concentrated in vacuo. The residue was purified by silica gel column chromatography to afford the desired product.

*4.9.1. 2-Chloro-5-nitroquinoline (**5**).* From **4**, procedure A, yield 30%, yellow solid; ^{1}H NMR (300 MHz, $CDCl_3$): δ 8.99 (d, J = 9.18 Hz, 1H), 8.40 (d, J = 7.68 Hz, 1H), 8.34 (d, J = 8.61 Hz, 1H), 7.84 (t, J = 8.13 Hz, 1H), 7.63 (d, J = 8.97 Hz, 1H).

*4.9.2. 2-Chloro-8-nitroquinoline (**6**).* From **4**, procedure A, yield 60%, yellow solid; ^{1}H NMR (400 MHz, $CDCl_3$): δ 8.19 (d, J = 8.6 Hz, 1H), 8.08 (dd, J = 7.3, 1.2 Hz, 1H), 8.02−8.04 (m, 1H), 7.62−7.66 (m, 1H), 7.52−7.54 (m, 1H).

*4.9.3. 5-Aminoquinolin-2(1H)-one (**7**).* From **5**, procedures D (method A) and F, yield 45% (in 2 steps), white solid; ^{1}H NMR (300 MHz, DMSO-d_6): δ 11.39 (s, 1H), 8.08 (d, J = 9.6 Hz, 1H), 7.10 (t, J = 8.0 Hz, 1H), 6.44 (d, J = 7.8 Hz, 1H), 6.33 (d, J = 7.8 Hz, 1H), 6.26 (d, J = 9.6 Hz, 1H), 5.86 (s, 2H).

*4.9.4. 5-Amino-1-methylquinolin-2(1H)-one (**8**).* From **5**, procedure D (method A), E and F, yield 62% (in 3 steps), white solid; ^{1}H NMR (300 MHz, DMSO-d_6): δ 8.09 (d, J = 9.7 Hz, 1H), 7.23 (t, J = 8.2 Hz, 1H), 6.55 (d, J = 8.2 Hz, 1H), 6.45 (d, J = 8.0 Hz, 1H), 6.37 (d, J = 9.7 Hz, 1H), 5.94 (s, 2H), 3.51 (s, 3H).

*4.9.5. Phenyl (2-Oxo-1,2-dihydroquinolin-5-yl)carbamate (**9**).* From **7**, procedure G, yield 91%, pale yellow solid; ^{1}H NMR (300 MHz, DMSO-d_6): δ 11.37 (s, 1H), 9.31 (s, 1H), 8.06 (d, J = 9.9 Hz, 1H), 7.16 (m, 3H), 6.73 (d, J = 8.0 Hz, 3H), 6.42 (d, J = 7.8 Hz, 1H), 6.32 (d, J = 7.8 Hz, 1H), 6.25 (d, J = 9.6 Hz, 1H).

*4.9.6. Phenyl (1-Methyl-2-oxo-1,2-dihydroquinolin-5-yl)-carbamate (**10**).* From **8**, procedure G, yield 93%, pale yellow solid; ^{1}H NMR (300 MHz, DMSO-d_6): δ 9.32 (s, 1H), 8.46 (d, J = 9.87 Hz, 1H), 7.81 (d, J = 8.2 Hz, 1H), 7.65 (d, J = 9.5 Hz, 1H), 7.53 (d, J = 7.6

https://dx.doi.org/10.1021/acs.jmedchem.0c00982
J. Med. Chem. 2021, 64, 370−384

Hz, 1H), 7.15 (t, J = 8.0 Hz, 2H), 6.76 (m, 3H), 6.42 (d, J = 7.8 Hz, 1H), 3.66 (s, 3H).

*4.9.7. 8-Aminoquinolin-2(1H)-one (**12**).* From **6**, procedures D (method A) and F, yield 61% (in 2 steps), white solid; ^{1}H NMR (400 MHz, DMSO-d_6): δ 10.80 (s, 1H), 7.76 (d, J = 9.8 Hz, 1H), 6.82−6.91 (m, 2H), 6.76 (dd, J = 7.7, 1.5 Hz, 1H), 6.40 (d, J = 9.8 Hz, 1H), 5.47 (s, 2H).

*4.9.8. Phenyl (2-Oxo-1,2-dihydroquinolin-8-yl)carbamate (**13**).* From **12**, procedure G, yield 93%, white solid;^{1}H NMR (400 MHz, DMSO-d_6): δ 9.27 (s, 1H), 7.98 (d, J = 9.8 Hz, 1H), 7.38 (d, J = 7.3 Hz, 1H), 7.27 (t, J = 7.6 Hz, 1H), 7.09−7.17 (m, 3H), 6.71 (t, J = 7.9 Hz, 3H), 6.56 (d, J = 9.8 Hz, 1H).

*4.9.9. 5-Nitroisoquinolin-1(2H)-one (**16**).* From **15**, procedures A and D (method A), yield 63% (in 2 steps), white solid; ^{1}H NMR (400 MHz, DMSO-d_6): δ 11.79 (s, 1H), 8.57 (d, J = 7.8 Hz, 1H), 8.46 (d, J = 6.0 Hz, 1H), 7.66 (t, J = 7.8 Hz, 1H), 7.45 (t, J = 7.5 Hz, 1H), 6.97 (d, J = 7.6 Hz, 1H).

*4.9.10. 5-Aminoisoquinoline-1(2H)-one (**17**).* From **16**, procedure F, yield 91%, white solid; ^{1}H NMR (400 MHz, DMSO-d_6): δ 11.03 (s, 1H), 7.38 (d, J = 7.8 Hz, 1H), 7.14 (t, J = 7.6 Hz, 1H), 7.01 (t, J = 5.6 Hz, 1H), 6.85 (d, J = 7.6 Hz, 1H), 6.66 (d, J = 7.5 Hz, 1H), 5.60 (s, 2H).

*4.9.11. 5-Amino-2-methylisoquinolin-1(2H)-one (**18**).* From **16**, procedures E and F, yield 65% (in 2 steps), pale yellow solid; ^{1}H NMR (400 MHz, DMSO-d_6): δ 7.37 (d, J = 7.6 Hz, 1H), 7.28 (d, J = 7.2 Hz, 1H), 7.11 (t, J = 8.0 Hz, 1H), 6.80 (d, J = 7.6 Hz, 1H), 6.68 (d, J = 7.6 Hz, 1H), 5.59 (s, 2H), 3.42 (s, 3H).

*4.9.12. 5-Bromo-8-nitroisoquinoline (**21**).* From **20**, procedures B and A, yield 32% (in 2 steps), yellow powder; ^{1}H NMR (300 MHz, $CDCl_3$): δ 10.01 (s, 1H), 8.84 (d, J = 5.8 Hz, 1H), 8.17 (m, 3H).

*4.9.13. 8-Aminoisoquinoline-1(2H)-one (**22**).* From **21**, procedures D (method B) and F, yield 45% (in 2 steps); ^{1}H NMR (300 MHz, $CDCl_3$): δ 11.92 (s, 1H), 7.71 (d, J = 9.1 Hz, 1H), 7.31 (t, J = 8.8 Hz, 1H), 6.86 (d, J = 8.1 Hz, 1H), 6.65 (d, J = 7.8 Hz, 1H), 6.44 (s, 2H), 6.18 (d, J = 9.1 Hz, 1H).

*4.9.14. 6-Nitroquinoline-2(1H)-one (**25**).* From **24**, procedure A, yield 41%, yellow powder;^{1}H NMR (300 MHz, DMSO-d_6): δ 8.41 (s, 1H), 8.05 (d, J = 9.3 Hz, 1H), 7.79 (d, J = 9.1 Hz, 1H), 7.18 (d, J = 9.1 Hz, 1H), 6.44 (d, J = 9.3 Hz, 1H).

*4.9.15. 7-Nitroisoquinolin-1(2H)-one (**28**).* From **27**, procedure A, yield 31%, yellow powder; ^{1}H NMR (400 MHz, $CDCl_3$): δ 9.78 (br s, 1H), 9.26 (d, J = 2.5 Hz, 1H), 8.45 (dd, J = 9.2, 2.5 Hz, 1H), 7.68 (d, J = 8.6 Hz, 1H), 6.61 (d, J = 7.4 Hz, 1H).

*4.9.16. 7-Nitroquinoline (**31**).* From **30**, procedures A and C, yield 42% (in 2 steps), pale brown solid; ^{1}H NMR (300 MHz, DMSO-d_6): δ 9.13 (d, J = 4.2 Hz, 1H), 8.82 (s, 1H), 8.60 (d, J = 7.6 Hz, 1H), 8.38 (d, J = 8.9 Hz, 1H), 8.30 (d, J = 8.9 Hz, 1H), 7.79 (d, J = 4.2 Hz, 1H).

*4.9.17. 7-Nitroquinoline-2(1H)-one (**32**).* From **31**, procedure D (method C), yield 57%, yellow solid; ^{1}H NMR (300 MHz, DMSO-d_6): δ 8.15 (s, 1H), 8.05 (d, J = 9.6 Hz, 1H), 7.93 (m, 2H), 6.70 (d, J = 9.5 Hz, 1H), 3.36 (*br* s, 1H).

*4.9.18. 1-((2-(4-Methylpiperidin-1-yl)-6-(trifluoromethyl)pyridin-3-yl)methyl)-3-(2-oxo-1,2-dihydro-quinolin-5-yl)urea (**2**).* From **9**, procedure H, yield 82%, white solid, mp = 253.6−254.9 °C; ^{1}H NMR (300 MHz, DMSO-d_6): δ 11.72 (s, 1H), 8.74 (s, 1H), 8.03 (d, J = 9.9 Hz, 1H), 7.82 (d, J = 7.7 Hz, 1H), 7.55 (d, J = 7.7 Hz, 1H), 7.44 (d, J = 7.7 Hz, 1H), 7.36 (t, J = 8.1 Hz, 1H), 7.02 (t, J = 5.7 Hz, 1H), 6.96 (d, J = 8.1 Hz, 1H), 6.50 (d, J = 9.9 Hz, 1H), 4.35 (d, J = 5.3 Hz, 2H), 2.75 (m, 2H), 1.70 (m, 2H), 1.54 (*br* s, 1H), 1.29 (m, 1H), 0.94 (d, J = 6.4 Hz, 3H); ^{13}C NMR (100 MHz, DMSO-d_6): δ 161.5, 160.6, 155.4, 139.7, 137.3, 136.3, 134.7, 130.9, 130.5, 123.0, 120.5, 120.3, 113.9, 113.8, 111.0, 109.6, 50.0, 33.8, 30.2, 21.8; HRMS (FAB): calcd for $C_{23}H_{25}F_3N_5O_2$ [M + H]$^+$, 460.1882; found, 460.1972.

*4.9.19. 1-((2-(4-Methylpiperidin-1-yl)-6-(trifluoromethyl)pyridin-3-yl)methyl)-3-(1-oxo-1,2-dihydro-isoquinolin-5-yl)urea (**3**).* From **17**, procedures G and H, yield 72% (in 2 steps), white solid, mp = 240.3−242.1 °C; ^{1}H NMR (300 MHz, DMSO-d_6): δ 11.32 (*br* s, 1H), 8.57 (s, 1H), 8.11 (d, J = 7.8 Hz, 1H), 7.89 (m, 2H), 7.47 (d, J = 7.8 Hz, 1H), 7.41 (t, J = 8.1 Hz, 1H), 7.26 (t, J = 7.2 Hz, 1H), 7.09 (t, J = 5.7 Hz, 1H), 6.68 (d, J = 7.5 Hz, 1H), 4.38 (d, J = 5.4 Hz, 2H), 3.34 (m, 2H), 2.83 (t, J = 11.7 Hz, 2H), 1.73 (d, J = 12.6 Hz, 2H), 1.55 (*br* s, 1H), 1.36 (m, 2H), 0.97 (d, J = 6.3 Hz, 3H); ^{13}C NMR (100 MHz, DMSO-d_6): δ 161.6, 160.6, 155.5, 137.4, 134.4, 131.0, 129.6, 128.4, 126.7, 126.0, 123.9, 121.0, 113.8, 98.9, 50.0, 33.8, 30.2, 21.8; HRMS (FAB): calcd for $C_{24}H_{25}F_3N_5O_2$ [M + H]$^+$, 460.1882; found, 460.1967.

*4.9.20. 1-(1-Methyl-2-oxo-1,2-dihydroquinolin-5-yl)-3-((2-(4-methylpiperidin-1-yl)-6-(trifluoromethyl)-pyridin-3-yl)methyl)urea (**11**).* From **10**, procedure H, yield 75%, white solid, mp = 214.9−215.7 °C; ^{1}H NMR (300 MHz, DMSO-d_6): δ 8.85 (s, 1H), 8.05 (d, J = 10.0 Hz, 1H), 7.84 (d, J = 7.6 Hz, 1H), 7.63 (d, J = 8.0 Hz, 1H), 7.60−7.40 (m, 2H), 7.19 (d, J = 8.4 Hz, 1H), 7.09 (t, J = 5.6 Hz, 1H), 6.64 (d, J = 9.9 Hz, 1H), 4.36 (m, 2H), 3.61 (s, 3H), 3.39 (m, 2H), 2.79 (m, 2H), 1.72 (m, 2H), 1.65−1.50(*br* s, 1H), 1.33 (m, 2H), 0.96 (d, J = 6.3 Hz, 3H); ^{13}C NMR (100 MHz, DMSO-d_6): δ 160.7, 160.6, 155.5, 140.5, 137.4, 136.8, 133.5, 130.9, 119.6, 115.0, 113.8, 112.1, 109.2, 50.0, 33.8, 30.2, 29.3, 21.8; HRMS (FAB): calcd for $C_{24}H_{27}F_3N_5O_2$ [M + H]$^+$, 474.2039; found, 474.2115.

*4.9.21. 1-((2-(4-Methylpiperidin-1-yl)-6-(trifluoromethyl)pyridin-3-yl)methyl)-3-(2-oxo-1,2-dihydroquinolin-8-yl)urea (**14**).* From **13**, procedure H, yield 68%, white solid, mp = 246.8−247.4 °C; ^{1}H NMR (300 MHz, DMSO-d_6): δ 10.90 (s, 1H), 8.47 (s, 1H), 7.94 (t, J = 9.9 Hz, 2H), 7.68 (*br*, s, 1H), 7.48 (dd, J = 7.5 Hz, 2H), 7.16 (t, J = 7.5 Hz, 1H), 6.82 (br s, 1H), 6.55 (d, J = 8.7 Hz, 1H), 4.35 (s, 2H), 3.41 (m, 2H), 2.82 (t, J = 11.7 Hz, 2H), 1.75 (d, J = 12 Hz, 2H), 1.56 (*br* s, 1H), 1.32 (d, J = 10.8 Hz, 2H), 0.97 (d, J = 6.0 Hz, 3H); ^{13}C NMR (100 MHz, DMSO-d_6): δ 161.7, 160.5, 155.7, 140.9, 137.4, 131.1, 123.1, 121.6, 120.0, 113.8, 50.0, 33.8, 30.2; HRMS (FAB): calcd for $C_{23}H_{25}F_3N_5O_2$ [M + H]$^+$, 460.1882; found, 460.1967.

*4.9.22. 1-(2-Methyl-1-oxo-1,2-dihydroisoquinolin-5-yl)-3-((2-(4-methylpiperidin-1-yl)-6-(trifluoromethyl)pyridin-3-yl)methyl)urea (**19**).* From **18**, procedures G and F, yield 81% (in 2 steps), white solid, mp = 245.9−247.6 °C; ^{1}H NMR (300 MHz, DMSO-d_6): δ 8.58 (s, 1H), 8.09 (d, J = 7.9 Hz, 1H), 7.68 (d, J = 7.9 Hz, 2H), 7.45 (m, 3H), 7.05 (m, 1H), 6.70 (d, J = 7.7 Hz, 1H), 4.36 (d, J = 5.7 Hz, 2H), 3.50 (s, 3H), 2.78 (m, 2H), 1.72 (m, 2H), 1.29 (m, 2H), 0.95 (d, J = 6.4 Hz, 3H); ^{13}C NMR (100 MHz, DMSO-d_6): δ 161.1, 160.6, 155.5, 137.4, 134.4, 133.1, 130.9, 128.6, 126.3, 126.0, 123.3, 120.9, 113.8, 99.1, 50.0, 36.3, 33.8, 30.2, 21.8; HRMS (FAB): calcd for $C_{23}H_{27}F_3N_5O_2$ [M + H]$^+$, 474.2039; found, 474.2115.

*4.9.23. 1-((2-(4-Methylpiperidin-1-yl)-6-(trifluoromethyl)pyridin-3-yl)methyl)-3-(1-oxo-1,2-dihydroisoquinolin-8-yl)urea (**23**).* From **22**, procedures G and H, yield 76% (in 2 steps), white solid, mp = 246.8−247.4 °C; ^{1}H NMR (300 MHz, DMSO-d_6): δ 11.92 (s, 1H), 8.99 (s, 1H), 7.73 (m, 3H), 7.45 (m, 3H), 7.24−6.89 (m, 3H), 6.42 (d, J = 9.5 Hz, 1H), 4.30 (d, J = 5.0 Hz, 2H), 2.77 (t, J = 12.3 Hz, 2H), 1.72 (d, J = 12.3 Hz, 2H), 1.66 (s, 1H), 1.29 (q, J = 12.5 Hz, 2H), 0.96 (d, J = 6.2 Hz, 3H); ^{13}C NMR (100 MHz, DMSO-d_6): δ 164.5, 160.6, 154.9, 142.9, 139.2, 137.5, 133.0, 131.0, 128.2, 123.0, 120.3, 117.8, 114.1, 113.7, 111.7, 106.4, 50.0, 33.8, 30.2, 21.8; HRMS (FAB): calcd for $C_{23}H_{25}F_3N_5O_2$ [M + H]$^+$, 460.1882; found, 460.1959.

*4.9.24. 1-((2-(4-Methylpiperidin-1-yl)-6-(trifluoromethyl)pyridin-3-yl)methyl)-3-(2-oxo-1,2-dihydroquinolin-6-yl)urea (**26**).* From **25**, procedures F, G, and H, yield 42% (in 3 steps), white solid, mp = 248.6−249.3 °C; ^{1}H NMR (300 MHz, DMSO-d_6): δ 11.58 (s, 1H), 9.25 (s, 1H), 7.77 (m, 3H), 7.44 (m, 2H), 7.27−7.15 (m, 2H), 6.42 (d, J = 9.5 Hz, 1H), 4.30 (d, J = 5.0 Hz, 2H), 2.77 (t, J = 12.3 Hz, 2H), 1.72 (d, J = 12.3 Hz, 2H), 1.66 (s, 1H), 1.29 (q, J = 12.5 Hz, 2H), 0.96 (d, J = 6.2 Hz, 3H); ^{13}C NMR (100 MHz, DMSO-d_6): δ 161.5, 160.5, 155.6, 140.0, 137.2, 134.8, 133.7, 131.4, 123.0, 122.2, 120.3, 119.2, 115.4, 115.3, 113.8, 50.0, 33.8, 30.2, 21.8; HRMS (FAB): calcd for $C_{23}H_{25}F_3N_5O_2$ [M + H]$^+$, 460.1882; found, 460.1975.

*4.9.25. 1-((2-(4-Methylpiperidin-1-yl)-6-(trifluoromethyl)pyridin-3-yl)methyl)-3-(1-oxo-1,2-dihydroisoquinolin-7-yl)urea (**29**).* From **28**, procedures F, G, and H, yield 57% (in 3 steps), white solid, mp = 247.6−248.1 °C; ^{1}H NMR (300 MHz, DMSO-d_6): δ 8.44 (dd, J = 8.6, 1.8 Hz, 1H), 7.70 (m, 2H), 7.48 (d, J = 8.8 Hz, 1H), 7.17 (d, J = 7.7 Hz, 1H), 6.90 (d, J = 7.1 Hz, 1H), 6.51 (d, J = 7.1 Hz, 1H), 4.42 (s, 2H), 3.37 (d, J = 12.8 Hz, 2H), 2.82 (t, J = 11.2 Hz, 2H), 1.69 (d, J = 11.6 Hz, 2H); ^{13}C NMR (100 MHz, DMSO-d_6): δ 161.5, 160.6, 155.2, 138.8, 137.3, 132.0, 131.1, 126.7, 126.4, 123.4, 113.7, 105.4, 50.0, 33.8, 30.2, 21.8; HRMS (FAB): calcd for $C_{23}H_{25}F_3N_5O_2$ [M + H]$^+$, 460.1882; found, 460.1967.

https://dx.doi.org/10.1021/acs.jmedchem.0c00982
J. Med. Chem. 2021, 64, 370−384

*4.9.26. 1-((2-(4-Methylpiperidin-1-yl)-6-(trifluoromethyl)pyridin-3-yl)methyl)-3-(2-oxo-1,2-dihydroquinolin-7-yl)urea (**33**).* From **32**, procedures F, G, and H, yield 63% (in 3 steps), pale yellow solid, mp = 248.1−249.3 °C; ^{1}H NMR (300 MHz, DMSO-d_6): δ 11.56 (s, 1H), 9.19 (s, 1H), 7.80 (d, J = 7.8 Hz, 1H), 7.75 (d, J = 9.3 Hz, 1H), 7.55 (s, 1H), 7.47 (d, J = 8.5 Hz, 1H), 7.45 (d, J = 9.9 Hz, 1H), 7.14 (dd, J = 8.5 Hz, 1.8 Hz, 1H), 6.90 (s, 1H), 6.27 (d, J = 9.5 Hz, 1H), 4.34 (d, J = 5.4 Hz, 1H), 3.44 (d, J = 12.4 Hz, 2H), 2.79 (t, J = 11.7 Hz, 2H), 1.73 (d, J = 10.8 Hz, 2H), 1.56 (m, 1H), 1.34−1.26 (m, 2H), 0.97 (d, J = 6.3 Hz, 3H); ^{13}C NMR (100 MHz, DMSO-d_6): δ 162.3, 160.6, 154.9, 142.3, 139.9, 139.8, 137.2, 131.0, 128.2, 123.0, 120.3, 118.5, 113.8, 112.6, 102.2, 50.0, 33.8, 30.2, 21.8; HRMS (FAB): calcd for $C_{23}H_{25}F_3N_5O_2$ $[M + H]^+$, 460.1882; found, 460.1964.

*4.9.27. 1-(2-Oxo-1,2-dihydroquinolin-5-yl)-3-((2-(piperidin-1-yl)-6-(trifluoromethyl)pyridin-3-yl)methyl)urea (**34**).* From **7**, procedures G and H, yield 61% (in 2 steps), white solid, mp = 265.1−267.0 °C; ^{1}H NMR (300 MHz, DMSO-d_6): δ 11.65 (s, 1H), 10.50 (s, 1H), 9.20 (m, 1H), 8.27 (d, J = 9.9 Hz, 1H), 7.86 (d, J = 7.7 Hz, 1H), 7.49 (d, J = 7.8 Hz, 1H), 7.43 (d, J = 7.6 Hz, 1H), 7.31 (t, J = 8.0 Hz, 1H), 6.89 (d, J = 7.8 Hz, 1H), 6.39 (d, J = 10.0 Hz, 1H), 4.29 (d, J = 5.4 Hz, 2H), 1.62 (m, 10H); HRMS (FAB): calcd for $C_{22}H_{23}F_3N_5O_2$ $[M + H]^+$, 446.1726; found, 446.1815.

*4.9.28. 1-((2-(4-Benzylpiperidin-1-yl)-6-(trifluoromethyl)pyridin-3-yl)methyl)-3-(2-oxo-1,2-dihydroquinolin-5-yl)urea (**35**).* From **7**, procedures G and H, yield 54% (in 2 steps), white solid, mp = 273.6−274.1 °C; ^{1}H NMR (300 MHz, DMSO-d_6): δ 11.72 (s, 1H), 8.77 (s, 1H), 8.04 (d, J = 9.8 Hz, 1H), 7.83 (d, J = 7.9 Hz, 1H), 7.55 (d, J = 7.5 Hz, 1H), 7.45 (d, J = 7.7 Hz, 1H), 7.37 (t, J = 8.2 Hz, 1H), 7.31−7.26 (m, 2H), 7.21−7.18 (m, 3H), 7.06 (m, 1H), 6.96 (d, J = 8.2 Hz, 1H), 6.51 (d, J = 10.9 Hz, 1H), 4.35 (d, J = 5.4 Hz, 2H), 3.45 (d, J = 12.9 Hz, 2H), 2.74 (t, J = 10.9 Hz, 2H), 2.57 (d, J = 6.6 Hz, 2H), 1.68 (d, J = 11.9 Hz, 2H), 1.70 (m, 1H), 1.37 (m, 2H); HRMS (FAB): calcd for $C_{29}H_{29}F_3N_5O_2$ $[M + H]^+$, 536.2195; found, 536.2272.

*4.9.29. 1-(2-Oxo-1,2-dihydroquinolin-5-yl)-3-((2-(pyrrolidin-1-yl)-6-(trifluoromethyl)pyridin-3-yl)methyl)urea (**36**).* From **7**, procedures G and H, yield 61% (in 2 steps), white solid, mp = 291.6−292.2 °C; ^{1}H NMR (300 MHz, DMSO-d_6): δ 11.72 (s, 1H), 8.69 (s, 1H), 8.04 (d, J = 9.8 Hz, 1H), 7.68 (d, J = 7.9 Hz, 1H), 7.58 (m, 1H), 7.37 (m, 1H), 7.11 (d, J = 7.9 Hz, 1H), 6.96 (d, J = 7.4 Hz, 1H), 6.52 (d, J = 7.4 Hz, 1H), 4.43 (d, J = 5.4 Hz, 2H), 3.54 (m, 4H), 1.89 (m, 4H); HRMS (FAB) calcd for $C_{21}H_{21}F_3N_5O_2$ $[M + H]^+$, 432.1569; found, 432.1689.

*4.9.30. 1-((2-(Dipropylamino)-6-(trifluoromethyl)pyridin-3-yl)methyl)-3-(2-oxo-1,2-dihydroquinolin-5-yl)urea (**37**).* From **7**, procedures G and H, yield 67% (in 2 steps), white solid, mp = 292.3−293.8 °C; ^{1}H NMR (300 MHz, DMSO-d_6): δ 11.72 (s, 1H), 8.81 (s, 1H), 8.06 (d, J = 9.9 Hz, 1H), 7.79 (d, J = 7.6 Hz, 1H), 7.54 (d, J = 3.5 Hz, 1H), 7.38−7.34 (m, 2H), 7.14 (m, 1H), 6.95 (d, J = 8.4 Hz, 1H), 6.49 (d, J = 9.9 Hz, 1H), 4.32 (d, J = 5.6 Hz, 2H), 3.17 (t, J = 6.2 Hz, 4H), 1.50 (m, 4H), 0.81 (t, J = 7.3 Hz, 6H); HRMS (FAB): calcd for $C_{23}H_{27}F_3N_5O_2$ $[M + H]^+$, 462.2039; found, 462.2111.

*4.9.31. 1-((2-Butoxy-6-(trifluoromethyl)pyridin-3-yl)methyl)-3-(2-oxo-1,2-dihydroquinolin-5-yl)urea (**38**).* From **7**, procedures G and H, yield 64% (in 2 steps), white solid, mp = 294.2−295.1 °C; ^{1}H NMR (300 MHz, DMSO-d_6): δ 11.72 (s, 1H), 8.76 (s, 1H), 8.05 (d, J = 9.87 Hz, 1H), 7.81 (d, J = 7.5 Hz, 1H), 7.58 (d, J = 8.0 Hz, 1H), 7.48 (d, J = 7.5 Hz, 1H), 7.37 (t, J = 8.0 Hz, 1H), 6.97−6.94 (m, 2H), 6.52 (d, J = 9.8 Hz, 1H), 4.38−4.32 (m, 4H), 1.73 (m, 2H), 1.45 (m, 2H), 0.93 (t, J = 7.5 Hz, 3H); HRMS (FAB) calcd for $C_{21}H_{22}F_3N_4O_3$ $[M + H]^+$, 435.1566; found, 435.1640.

*4.9.32. 1-(2-Oxo-1,2-dihydroquinolin-5-yl)-3-((2-(pentyloxy)-6-(trifluoromethyl)pyridin-3-yl)methyl)urea (**39**).* From **7**, procedures G and H, yield 59% (in 2 steps), white solid, mp = 276.3−277.8 °C; ^{1}H NMR (300 MHz, DMSO-d_6): δ 11.72 (s, 1H), 8.76 (s, 1H), 8.05 (d, J = 9.8 Hz, 1H), 7.81 (d, J = 7.5 Hz, 1H), 7.58 (d, J = 8.0 Hz, 1H), 7.48 (d, J = 7.5 Hz, 1H), 7.37 (t, J = 8.0 Hz, 1H), 6.97−6.94 (m, 2H), 6.52 (d, J = 9.87 Hz, 1H), 4.37−4.32 (m, 4H), 1.77 (m, 2H), 1.46−1.28 (m, 4H), 0.88 (t, J = 7.14 Hz, 3H); HRMS (ESI): calcd for $C_{22}H_{23}F_3N_4O_3$ $[M + H]^+$, 448.1722; found, 449.1799.

*4.9.33. 1-((2-(Hexyloxy)-6-(trifluoromethyl)pyridin-3-yl)methyl)-3-(2-oxo-1,2-dihydroquinolin-5-yl)urea (**40**).* From **7**, procedures G and H, yield 62% (in 2 steps), white solid, mp = 285.4−286.2 °C; ^{1}H NMR (300 MHz, DMSO-d_6): δ 11.71 (s, 1H), 8.75 (s, 1H), 8.04 (d, J = 9.8 Hz, 1H), 7.80 (d, J = 7.5 Hz, 1H), 7.57 (d, J = 8.0 Hz, 1H), 7.46 (d, J = 7.5 Hz, 1H), 7.35 (t, J = 8.0 Hz, 1H), 6.95−6.93 (m, 2H), 6.51 (d, J = 9.8 Hz, 1H), 4.35−4.30 (m, 4H), 1.74 (m, 2H), 1.41 (m, 2H), 1.30−1.25 (m, 4H), 0.83 (t, J = 6.7 Hz, 3H); HRMS (FAB): calcd for $C_{23}H_{26}F_3N_4O_3$ $[M + H]^+$, 463.1879; found, 463.1957.

*4.9.34. 1-((2-Isobutoxy-6-(trifluoromethyl)pyridin-3-yl)methyl)-3-(2-oxo-1,2-dihydroquinolin-5-yl)urea (**41**).* From **7**, procedures G and H, yield 67% (in 2 steps), white solid, mp = 278.8−280.5 °C; ^{1}H NMR (300 MHz, DMSO-d_6): δ 11.71 (s, 1H), 8.75 (s, 1H), 8.04 (d, J = 9.5 Hz, 1H), 7.79 (m, 1H), 7.56 (d, J = 7.8 Hz, 1H), 7.47 (d, J = 6.6 Hz, 1H), 7.35 (m, 1H), 6.95 (m, 2H), 6.50 (d, J = 10.2 Hz, 1H), 4.34 (m, 2H), 4.11 (d, J = 6.0 Hz, 2H), 0.99 (d, J = 5.8 Hz, 6H); HRMS (FAB): calcd for $C_{21}H_{22}F_3N_4O_3$ $[M + H]^+$, 435.1566; found, 435.1634.

*4.9.35. 1-((2-(Cyclobutylmethoxy)-6-(trifluoromethyl)pyridin-3-yl)methyl)-3-(2-oxo-1,2-dihydroquinolin-5-yl)urea (**42**).* From **7**, procedures G and H, yield 71% (in 2 steps), white solid, mp = 271.2−272.1 °C; ^{1}H NMR (300 MHz, DMSO-d_6): δ 11.71 (s, 1H), 8.76 (s, 1H), 8.04 (d, J = 9.8 Hz, 1H), 7.79 (d, J = 7.6 Hz, 1H), 7.56 (d, J = 8.0 Hz, 1H), 7.47 (d, J = 7.3 Hz, 1H), 7.35 (t, J = 8.0 Hz, 1H), 6.95−6.92 (m, 2H), 6.50 (d, J = 9.8 Hz, 1H), 4.32−4.30 (m, 4H), 2.75 (m, 1H), 2.04 (m, 2H), 1.87 (m, 4H); HRMS (FAB): calcd for $C_{22}H_{22}F_3N_4O_3$ $[M + H]^+$, 447.1566; found, 447.1640.

*4.9.36. 1-((2-(Cyclopentylmethoxy)-6-(trifluoromethyl)pyridin-3-yl)methyl)-3-(2-oxo-1,2-dihydroquinolin-5-yl)urea (**43**).* From **7**, procedures G and H, yield 68% (in 2 steps), white solid, mp = 273.6−275.1 °C; ^{1}H NMR (300 MHz, DMSO-d_6): δ 11.71 (s, 1H), 8.76 (s, 1H), 8.04 (d, J = 9.8 Hz, 1H), 7.80 (d, J = 7.3 Hz, 1H), 7.56 (d, J = 8.0 Hz, 1H), 7.47 (d, J = 7.3 Hz, 1H), 7.36 (t, J = 8.0 Hz, 1H), 6.96−6.93 (m, 2H), 6.50 (d, J = 9.8 Hz, 1H), 4.32 (d, J = 5.8 Hz, 2H), 4.22 (d, J = 6.9 Hz, 2H), 2.36 (m, 1H), 1.75 (m, 2H), 1.56 (m, 4H), 1.36 (m, 2H); HRMS (FAB): calcd for $C_{23}H_{24}F_3N_4O_3$ $[M + H]^+$, 461.1722; found, 461.1795.

*4.9.37. 1-((2-(Benzyloxy)-6-(trifluoromethyl)pyridin-3-yl)methyl)-3-(2-oxo-1,2-dihydroquinolin-5-yl)urea (**44**).* From **7**, procedures G and H, yield 61% (in 2 steps), white solid, mp = 275.1−276.2 °C; ^{1}H NMR (300 MHz, DMSO-d_6): δ 11.73 (s, 1H), 8.77 (s, 1H), 8.04 (d, J = 10.2 Hz, 1H), 7.85 (d, J = 7.5 Hz, 1H), 7.52−7.59 (m, 3H), 7.32−7.39 (m, 5H), 7.00 (m, 1H), 6.51 (d, J = 10.4 Hz, 1H), 5.45 (s, 1H), 4.37 (m, 2H); HRMS (FAB): calcd for $C_{24}H_{20}F_3N_4O_3$ $[M + H]^+$, 469.1409; found, 469.1497.

*4.9.38. 1-((2-(Cyclohexylthio)-6-(trifluoromethyl)pyridin-3-yl)methyl)-3-(2-oxo-1,2-dihydroquinolin-5-yl)urea (**45**).* From **7**, procedures G and H, yield 77% (in 2 steps), white solid, mp = 276.2−279.4 °C; ^{1}H NMR (400 MHz, DMSO-d_6): δ 11.70 (s, 1H), 8.79 (s, 1H), 8.06 (d, J = 9.8 Hz, 1H), 7.79 (d, J = 7.7 Hz, 1H), 7.62 (d, J = 7.8 Hz, 1H), 7.56 (d, J = 7.9 Hz, 1H), 7.36 (t, J = 8.1 Hz, 1H), 7.07 (t, J = 5.6 Hz, 1H), 6.96 (d, J = 8.1 Hz, 1H), 6.51 (d, J = 9.8 Hz, 1H), 4.27 (d, J = 5.4 Hz, 2H), 3.91 (m, 1H), 2.06 (m, 2H), 1.74 (m, 2H), 1.61−1.29 (m, 6H); HRMS (FAB): calcd for $C_{23}H_{24}F_3N_4O_2S$ $[M + H]^+$, 477.1494; found, 477.1521.

*4.9.39. 1-((2-(4-Methylcyclohexyl)-6-(trifluoromethyl)pyridin-3-yl)methyl)-3-(2-oxo-1,2-dihydroquinolin-5-yl)urea (**46**).* From **7**, procedures G and H, yield 62% (in 2 steps), white solid, mp = 280.3−282.5 °C; ^{1}H NMR (300 MHz, DMSO-d_6): δ 11.72 (s, 1H), 8.70 (s, 1H), 8.01 (d, J = 9.7 Hz, 1H), 7.89 (d, J = 8.0 Hz, 1H), 7.70 (d, J = 7.8 Hz, 1H), 7.55 (d, J = 8.0 Hz, 1H), 7.37 (t, J = 8.0 Hz, 1H), 7.01 (m, 1H), 6.96 (d, J = 8.0 Hz, 1H), 6.51 (d, J = 9.6 Hz, 1H), 4.49 (d, J = 5.4 Hz, 2H), 3.06 (m, 1H), 1.85−1.54 (m, 9H), 1.02−0.90 (m, 3H); HRMS (FAB): calcd for $C_{24}H_{26}F_3N_4O_2$ $[M + H]^+$, 459.1930; found, 459.2003.

*4.9.40. 1-((2-(3-Isopropylphenyl)-6-(trifluoromethyl)pyridin-3-yl)methyl)-3-(2-oxo-1,2-dihydroquinolin-5-yl)urea (**47**).* From **7**, procedures G and H, yield 58% (in 2 steps), white solid, mp = 281.3−282.7 °C; ^{1}H NMR (300 MHz, DMSO-d_6): δ 11.72 (s, 1H), 8.72 (s, 1H), 8.12 (d, J = 8.1 Hz, 1H), 7.98 (m, 2H), 7.42 (m, 6H), 7.12 (s, 1H), 6.96 (d, J = 8.1 Hz, 1H), 6.51 (d, J = 9.9 Hz, 1H), 4.42 (d, J = 5.4 Hz, 2H), 2.98 (m, 1H), 1.24 (d, J = 6.9 Hz, 6H); HRMS (FAB): calcd for $C_{26}H_{24}F_3N_4O_2$ $[M + H]^+$, 481.1773; found, 481.1790.

*4.9.41. 1-((2-(4-Fluorophenyl)-6-(trifluoromethyl)pyridin-3-yl)methyl)-3-(2-oxo-1,2-dihydroquinolin-5-yl)urea (**48**).* From **7**, pro-

https://dx.doi.org/10.1021/acs.jmedchem.0c00982
J. Med. Chem. 2021, 64, 370−384

cedures G and H, yield 61% (in 2 steps), white solid, mp = 268.5−269.2 °C; ^{1}H NMR (400 MHz, DMSO-d_6): δ 11.69 (s, 1H), 8.73 (s, 1H), 8.13 (d, J = 8.0 Hz, 1H), 8.00 (d, J = 9.8 Hz, 1H), 7.94 (d, J = 7.9 Hz, 1H), 7.68−7.64 (m, 2H), 7.49 (d, J = 7.8 Hz, 1H), 7.39−7.33 (m, 3H), 7.09 (t, J = 5.5 Hz, 1H), 6.95 (d, J = 8.1 Hz, 1H), 6.50 (d, J = 9.8 Hz, 1H), 4.43 (d, J = 5.4 Hz, 2H); HRMS (FAB): calcd for $C_{23}H_{17}F_4N_4O_2$ $[M + H]^+$, 457.1209; found, 457.1286.

*4.9.42. 1-((1-(3-Chlorophenyl)-3-(trifluoromethyl)-1H-pyrazol-5-yl)methyl)-3-(2-oxo-1,2-dihydroquinolin-5-yl)urea (**49**).* From **7**, procedures G and H, yield 60% (in 2 steps), white solid, mp = 269.5−270.3 °C; ^{1}H NMR (300 MHz, CD_3OD): δ 8.66 (d, J = 8.1 Hz, 1H), 8.44 (d, J = 7.5 Hz, 1H), 7.66 (t, J = 8.1 Hz, 1H), 7.39 (d, J = 7.5 Hz, 1H), 7.21 (d, J = 7.0 Hz, 1H); HRMS (FAB): calcd for $C_{21}H_{16}ClF_3N_5O_2$ $[M + H]^+$, 462.0866; found, 462.0940.

*4.9.43. 1-((1-(3-Fluorophenyl)-3-(trifluoromethyl)-1H-pyrazol-5-yl)methyl)-3-(2-oxo-1,2-dihydroquinolin-5-yl)urea (**50**).* From **7**, procedures G and H, yield 71% (in 2 steps), white solid, mp = 294.9−295.7 °C; ^{1}H NMR (300 MHz, DMSO-d_6): δ 11.74 (s, 1H), 8.63 (s, 1H), 7.98 (d, J = 9.9 Hz, 2H), 7.65 (m, 2H), 7.45 (m, 4H), 6.99 (m, 2H), 6.88 (s, 1H), 6.52 (d, J = 9.6 Hz, 1H), 4.48 (d, J = 5.7 Hz, 2H); HRMS (FAB): calcd for $C_{21}H_{16}F_4N_5O_2$ $[M + H]^+$, 446.1162; found, 446.1238.

*4.9.44. 1-(2-Oxo-1,2-dihydroquinolin-5-yl)-3-((1-(m-tolyl)-3-(trifluoromethyl)-1H-pyrazol-5-yl)methyl)urea (**51**).* From **7**, procedures G and H, yield 63% (in 2 steps), white solid, mp = 294.2−295.6 °C; ^{1}H NMR (300 MHz, DMSO-d_6): δ 11.7 (s, 1H), 8.65 (s, 1H), 7.98 (d, J = 9.9 Hz, 1H), 7.45 (m, 6H), 7.03 (t, J = 5.7 Hz, 1H), 6.97 (d, J = 8.1 Hz, 1H), 6.82 (s, 1H), 6.50 (d, J = 9.9 Hz, 1H), 4.41 (d, J = 5.7 Hz, 2H), 2.48 (s, 3H); HRMS (FAB): calcd for $C_{22}H_{19}F_3N_5O_2$ $[M + H]^+$, 442.1413; found, 442.1479.

*4.9.45. 1-((1-(3-Isopropylphenyl)-3-(trifluoromethyl)-1H-pyrazol-5-yl)methyl)-3-(2-oxo-1,2-dihydroquinolin-5-yl)urea (**52**).* From **7**, procedures G and H, yield 56% (in 2 steps), white solid, mp = 253.6−254.1 °C; ^{1}H NMR (300 MHz, DMSO-d_6): δ 11.72 (s, 1H), 8.65 (s, 1H), 7.98 (d, J = 9.9 Hz, 1H), 7.49 (m, 6H), 7.03 (t, J = 5.1 Hz, 1H), 6.96 (d, J = 1.2 Hz, 1H), 6.85 (s, 1H), 6.50 (d, J = 9.9 Hz, 1H), 4.41 (d, J = 5.4 Hz, 2H), 3.00 (m, 1H), 1.22 (d, J = 6.2 Hz, 6H); HRMS (FAB): calcd for $C_{24}H_{23}F_3N_5O_2$ $[M + H]^+$, 470.1726; found, 470.1799.

*4.9.46. 1-((3-(tert-Butyl)-1-(3-chlorophenyl)-1H-pyrazol-5-yl)methyl)-3-(2-oxo-1,2-dihydroquinolin-5-yl)urea (**53**).* From **7**, procedures G and H, yield 54% (in 2 steps), white solid, mp = 257.1−258.3 °C; ^{1}H NMR (300 MHz, DMSO-d_6): δ 11.72 (s, 1H), 8.56 (s, 1H), 7.98 (d, J = 9.9 Hz, 1H), 7.52 (m, 5H), 7.30 (t, J = 7.8 Hz, 1H), 6.98 (d, J = 8.1 Hz, 1H), 6.92 (t, J = 5.4 Hz, 1H), 6.51 (d, J = 9.9 Hz, 1H), 6.37 (s, 1H), 4.45 (d, J = 5.4 Hz, 2H), 1.29 (s, 9H); HRMS (FAB): calcd for $C_{24}H_{25}ClN_5O_2$ $[M + H]^+$, 450.1619; found, 450.1630.

*4.9.47. 1-((3-(tert-Butyl)-1-(3-fluorophenyl)-1H-pyrazol-5-yl)methyl)-3-(2-oxo-1,2-dihydroquinolin-5-yl)urea (**54**).* From **7**, procedures G and H, yield 63% (in 2 steps), white solid, mp = 250.9−251.2 °C; ^{1}H NMR (300 MHz, DMSO-d_6): δ 11.72 (s, 1H), 8.74 (s, 1H), 8.03 (d, J = 9.9 Hz, 1H), 7.82 (d, J = 7.7 Hz, 1H), 7.55 (d, J = 7.7 Hz, 1H), 7.44 (d, J = 7.7 Hz, 1H), 7.36 (t, J = 8.1 Hz, 1H), 7.02 (t, J = 5.7 Hz, 1H), 6.96 (d, J = 8.1 Hz, 1H), 6.50 (d, J = 9.9 Hz, 1H), 4.35 (d, J = 5.3 Hz, 2H), 2.75 (m, 2H), 1.70 (m, 2H), 1.54 (*br* s, 1H), 1.29 (m, 1H), 0.94 (d, J = 6.4 Hz, 3H); HRMS (FAB): calcd for $C_{24}H_{25}FN_5O_2$ $[M + H]^+$, 434.1914; found, 434.1989.

*4.9.48. 1-(1-Oxo-1,2-dihydroisoquinolin-5-yl)-3-((2-(piperidin-1-yl)-6-(trifluoromethyl)pyridin-3-yl)methyl)urea (**55**).* From **17**, procedures G and H, yield 61% (in 2 steps), white solid, mp = 231.2−232.3 °C; ^{1}H NMR (300 MHz, DMSO-d_6): δ 11.32 (d, J = 5.3 Hz, 1H), 8.58 (s, 1H), 8.10 (d, J = 6.7 Hz, 1H), 7.87 (d, J = 8.3 Hz, 1H), 7.84 (d, J = 8.2 Hz, 1H), 7.47 (d, J = 7.7 Hz, 1H), 7.38 (t, J = 8.0 Hz, 1H), 7.24 (t, J = 7.7 Hz, 1H), 7.09 (t, J = 7.7 Hz, 1H), 6.67 (d, J = 7.5 Hz, 1H), 4.37 (d, J = 5.9 Hz, 2H), 3.11 (m, 4H), 1.67 (m, 6H); HRMS (FAB): calcd for $C_{22}H_{22}F_3N_5O_2$ $[M + H]^+$, 446.1726; found, 446.1790.

*4.9.49. 1-((2-(4-Benzylpiperidin-1-yl)-6-(trifluoromethyl)pyridin-3-yl)methyl)-3-(1-oxo-1,2-dihydroisoquinolin-5-yl)urea (**56**).* From **17**, procedures G and H, yield 60% (in 2 steps), white solid, mp = 231.8−232.1 °C; ^{1}H NMR (300 MHz, DMSO-d_6): δ 11.34 (d, J = 4.9 Hz, 1H), 8.58 (s, 1H), 8.09 (d, J = 7.1 Hz, 1H), 7.89−7.82 (m, 2H), 7.46 (d, J = 7.8 Hz, 1H), 7.38 (t, J = 8.0 Hz, 1H), 7.31−7.28 (m, 4H), 7.18 (bt, 1H), 6.67 (d, J = 7.1 Hz, 1H), 4.36 (d, J = 5.4 Hz, 2H), 3.45 (d, J = 12.4 Hz, 2H), 2.74 (d, J = 12.0 Hz, 2H), 2.7 (m, 1H), 1.70−1.66 (m, 3H), 1.35 (m, 2H); HRMS (FAB): calcd for $C_{29}H_{29}F_3N_5O_2$ $[M + H]^+$, 536.2195, found, 536.2264.

*4.9.50. 1-(1-Oxo-1,2-dihydroisoquinolin-5-yl)-3-((2-(pyrrolidin-1-yl)-6-(trifluoromethyl)pyridin-3-yl)methyl)urea (**57**).* From **17**, procedures G and H, yield 60% (in 2 steps), white solid, mp = 230.8−231.2 °C; ^{1}H NMR (300 MHz, DMSO-d_6): δ 11.31 (d, J = 5.3 Hz, 1H), 8.83 (s, 1H), 8.16 (dd, J = 7.9, 1.2 Hz, 1H), 7.85 (d, J = 7.5 Hz, 1H), 7.72 (d, J = 7.7 Hz, 1H), 7.45 (t, J = 5.6 Hz, 1H), 7.37 (t, J = 8.0 Hz, 1H), 7.19 (m, 1H), 7.12 (d, J = 7.6 Hz, 1H), 6.85 (d, J = 7.5 Hz, 1H), 4.44 (d, J = 5.4 Hz, 2H), 3.55 (t, J = 6.6 Hz, 4H), 1.90 (m, 4H); HRMS (FAB): calcd for $C_{21}H_{21}F_3N_5O_2$ $[M + H]^+$, 432.1569; found, 432.1589.

*4.9.51. 1-((2-(Dipropylamino)-6-(trifluoromethyl)pyridin-3-yl)methyl)-3-(1-oxo-1,2-dihydroisoquinolin-5-yl)urea (**58**).* From **17**, procedures G and H, yield 75% (in 2 steps), white solid, mp = 214.4−216.7 °C; ^{1}H NMR (300 MHz, DMSO-d_6): δ 11.34 (d, J = 5.3 Hz, 1H), 8.56 (s, 1H), 8.10 (d, J = 7.9 Hz, 1H), 7.87 (d, J = 7.9 Hz, 1H), 7.81 (d, J = 7.7 Hz, 1H), 7.38 (t, J = 7.5 Hz, 2H), 7.25 (t, J = 7.3 Hz, 1H), 7.07 (t, J = 5.7 Hz, 1H), 6.67 (d, J = 7.5 Hz, 1H), 4.35 (d, J = 5.7 Hz, 2H), 3.19 (t, J = 7.0 Hz, 4H), 1.45−1.57 (m, 4H), 0.83 (t, J = 7.3 Hz, 6H); HRMS (FAB): calcd for $C_{23}H_{27}F_3N_5O_2$ $[M + H]^+$, 462.2039; found, 462.2115.

*4.9.52. 1-((2-Butoxy-6-(trifluoromethyl)pyridin-3-yl)methyl)-3-(1-oxo-1,2-dihydroisoquinolin-5-yl)urea (**59**).* From **17**, procedures G and H, yield 59% (in 2 two steps), white solid, mp = 212.9−213.2 °C; ^{1}H NMR (300 MHz, DMSO-d_6): δ 11.29 (s, 1H), 8.56 (s, 1H), 8.11 (d, J = 7.0 Hz, 1H), 7.87 (d, J = 8.1 Hz, 1H), 7.82 (d, J = 7.5 Hz, 1H), 7.69 (m, 1H), 7.48 (d, J = 7.5 Hz, 1H), 7.38 (t, J = 8.0 Hz, 1H), 7.23 (t, J = 7.0 Hz, 1H), 7.00 (m, 1H), 6.68 (d, J = 7.1 Hz, 1H), 4.35 (m, 4H), 1.70−1.79 (m, 2H), 1.42−1.49 (m, 2H), 0.93 (t, J = 7.3 Hz, 3H); HRMS (FAB): calcd for $C_{21}H_{22}F_3N_4O_3$ $[M + H]^+$, 435.1566; found, 435.1578.

*4.9.53. 1-((2-Isobutoxy-6-(trifluoromethyl)pyridin-3-yl)methyl)-3-(1-oxo-1,2-dihydroisoquinolin-5-yl)urea (**60**).* From **17**, procedures G and H, yield 63% (in 2 steps), white solid, mp = 213.8−214.3 °C; ^{1}H NMR (300 MHz, DMSO-d_6): δ 11.33 (d, J = 5.1 Hz, 1H), 8.63 (s, 1H), 8.12 (dd, J = 7.8, 1.1 Hz, 1H), 7.87 (d, J = 7.5 Hz, 1H), 7.83 (d, J = 7.5 Hz, 1H), 7.49 (d, J = 7.3 Hz, 1H), 7.38 (d, J = 7.5 Hz, 1H), 7.49 (d, J = 7.3 Hz, 1H), 7.38 (t, J = 7.8 Hz, 1H), 7.23 (t, J = 5.8 Hz, 1H), 7.07 (t, J = 5.8 Hz, 1H), 6.07 (d, J = 7.3 Hz, 1H), 4.35 (d, J = 5.4 Hz, 2H), 4.13 (d, J = 6.3 Hz, 2H), 2.09 (p, J = 6.6 Hz, 1H), 1.01 (d, J = 6.6 Hz, 6H); HRMS (FAB): calcd for $C_{21}H_{22}F_3N_4O_3$ $[M + H]^+$, 435.1566; found, 435.1578.

*4.9.54. 1-((2-(Cyclobutylmethoxy)-6-(trifluoromethyl)pyridin-3-yl)methyl)-3-(1-oxo-1,2-dihydroisoquinolin-5-yl)urea (**61**).* From **17**, procedures G and H, yield 74% (in 2 steps), white solid, mp = 213.8−214.2 °C; ^{1}H NMR (300 MHz, DMSO-d_6): δ 11.33 (d, J = 5.4 Hz, 1H), 8.59 (s, 1H), 8.12 (d, J = 6.7 Hz, 1H), 7.87 (d, J = 7.8 Hz, 1H), 7.82 (d, J = 7.5 Hz, 1H), 7.49 (d, J = 7.5 Hz, 1H), 7.38 (t, J = 8.0 Hz, 1H), 7.24 (d, J = 5.8 Hz, 1H), 7.00 (t, J = 5.6 Hz, 1H), 4.33 (d, J = 6.6 Hz, 4H), 2.77 (m, 1H), 2.10−1.99 (m, 6H); HRMS (FAB): calcd for $C_{22}H_{22}F_3N_4O_3$ $[M + H]^+$, 447.1566; found, 447.1579.

*4.9.55. 1-((2-(Cyclopentylmethoxy)-6-(trifluoromethyl)pyridin-3-yl)methyl)-3-(1-oxo-1,2-dihydroisoquinolin-5-yl)urea (**62**).* From **17**, procedures G and H, yield 76% (in 2 steps), white solid, mp = 232.3−234.1 °C; ^{1}H NMR (300 MHz, DMSO-d_6): δ 11.33 (s, 1H), 8.60 (s, 1H), 8.10 (d, J = 6.9 Hz, 1H), 7.85 (d, J = 7.8 Hz, 1H), 7.80 (d, J = 7.5 Hz, 1H), 7.47 (d, J = 7.5 Hz, 1H), 7.36 (t, J = 7.8 Hz, 1H), 7.23 (t, J = 5.6 Hz, 1H), 7.02 (t, J = 6.0 Hz, 1H), 6.68 (d, J = 7.5 Hz, 1H), 4.32 (d, J = 5.4 Hz, 2H), 4.22 (d, J = 6.9 Hz, 2H), 2.34 (p, J = 7.3 Hz, 1H), 1.78−1.76 (m, 2H), 1.60−1.48 (m, 4H), 1.38−1.32 (m, 2H); HRMS (FAB): calcd for $C_{23}H_{24}F_3N_4O_3$ $[M + H]^+$, 461.1722; found, 461.1787.

*4.9.56. 1-((2-(Benzyloxy)-6-(trifluoromethyl)pyridin-3-yl)methyl)-3-(1-oxo-1,2-dihydroisoquinolin-5-yl)urea (**63**).* From **17**, procedures G and H, yield 81% (in 2 steps), white solid, mp = 231.6−232.6 °C; ^{1}H NMR (300 MHz, DMSO-d_6): δ 11.30 (s, 1H), 8.59 (s, 1H), 8.11 (d, J = 7.7 Hz, 1H), 7.87 (d, J = 8.1 Hz, 2H), 7.54 (m, 4H), 7.32−7.40 (m, 4H), 7.23 (t, J = 7.3 Hz, 1H), 7.06 (m, 1H), 6.68 (d, J = 7.3 Hz, 1H), 5.46 (s, 2H), 4.38 (d, J = 5.7 Hz, 2H); HRMS (FAB): calcd for $C_{24}H_{20}F_3N_4O_3$ $[M + H]^+$, 469.1409; found, 469.1501.

*4.9.57. 1-((2-(Cyclohexylthio)-6-(trifluoromethyl)pyridin-3-yl)methyl)-3-(1-oxo-1,2-dihydroisoquinolin-5-yl)urea (**64**).* From **17**,

https://dx.doi.org/10.1021/acs.jmedchem.0c00982
J. Med. Chem. 2021, 64, 370−384

procedures G and H, yield 54% (in 2 steps), white solid, mp = 264.8−265.4 °C; ^{1}H NMR (300 MHz, DMSO-d_6): δ 11.31 (*br* s, 1H), 8.63 (s, 1H), 8.10 (d, J = 7.8 Hz, 1H), 7.88 (d, J = 8.0 Hz, 1H), 7.79 (d, J = 7.6 Hz, 1H), 7.63 (d, J = 7.8 Hz, 1H), 7.38 (t, J = 8.0 Hz, 1H), 7.24 (t, J = 6.5 Hz, 1H), 7.12 (bt, 1H), 6.69 (d, J = 7.5 Hz, 1H), 4.28 (d, J = 5.4 Hz, 2H), 3.92 (m, 1H), 2.05−1.94 (m, 4H), 1.58−1.23 (m, 6H); HRMS (FAB): calcd for $C_{23}H_{24}F_3N_4O_2S$ $[M + H]^+$, 477.1494; found, 477.1513.

*4.9.58. 1-((2-(3-Isopropylphenyl)-6-(trifluoromethyl)pyridin-3-yl)-methyl)-3-(1-oxo-1,2-dihydroisoquinolin-5-yl)urea (**65**).* From **17**, procedures G and H, yield 68% (in 2 steps), white solid, mp = 287.2−288.4 °C; ^{1}H NMR (300 MHz, DMSO-d_6): δ 11.30 (s, 1H), 8.54 (s, 1H), 8.12 (d, J = 8.0 Hz, 1H), 8.03 (dd, J = 7.9, 1.2 Hz, 1H), 7.92 (d, J = 8.0 Hz, 1H), 7.85 (d, J = 7.5 Hz, 1H), 7.46−7.32 (m, 5H), 7.21 (t, J = 7.3 Hz, 1H), 7.10 (*bt*, 1H), 6.53 (d, J = 7.3 Hz, 2H), 4.42 (d, J = 5.4 Hz, 2H), 2.97 (p, J = 6.7 Hz, 1H), 1.23 (d, J = 6.9 Hz, 6H); HRMS (FAB): calcd for $C_{26}H_{24}F_3N_4O_2$ $[M + H]^+$, 481.1773; found, 481.1842.

*4.9.59. 1-((1-(3-Chlorophenyl)-3-(trifluoromethyl)-1H-pyrazol-5-yl)methyl)-3-(1-oxo-1,2-dihydroisoquinolin-5-yl)urea (**66**).* From **17**, procedures G and H, yield 71% (in 2 steps), white solid, mp = 229.0−231.2 °C; ^{1}H NMR (300 MHz, DMSO-d_6): δ 11.31 (*br* s, 1H), 8.45 (s, 1H), 8.03 (d, J = 8.1 Hz, 1H), 7.89 (d, J = 8.1 Hz, 1H), 7.76 (s, 1H), 7.36 (s, 3H), 7.30 (t, J = 8.1 Hz, 1H), 7.24 (t, J = 7.2 Hz, 1H), 7.03 (t, J = 5.7 Hz, 1H), 6.88 (s, 1H), 6.61 (d, J = 7.5 Hz, 1H), 4.48 (d, J = 5.4 Hz, 2H); HRMS (FAB): calcd for $C_{21}H_{16}ClF_3N_5O_2$ $[M + H]^+$, 462.0866; found, 462.0939.

*4.9.60. 1-((3-(tert-Butyl)-1-(3-chlorophenyl)-1H-pyrazol-5-yl)-methyl)-3-(1-oxo-1,2-dihydroisoquinolin-5-yl)urea (**67**).* From **17**, procedures G and H, yield 81% (in 2 steps), white solid, mp = 224.8−225.1 °C; ^{1}H NMR (300 MHz, DMSO-d_6): δ 11.32 (*br* s, 1H), 8.39 (s, 1H), 8.10 (d, J = 7.8 Hz, 1H), 7.88 (d, J = 7.8 Hz, 1H), 7.57 (s, 1H), 7.51 (m, 3H), 7.38 (t, J = 8.1 Hz, 1H), 7.24 (d, J = 7.2 Hz, 1H), 7.18 (t, J = 8.7 Hz, 1H), 6.97 (t, J = 5.7 Hz, 1H), 6.78 (m, 1H), 6.62 (d, J = 7.5 Hz, 1H), 6.38 (s, 1H), 4.45 (d, J = 5.1 Hz, 2H), 1.29 (s, 9H); HRMS (FAB): calcd for $C_{24}H_{25}ClN_5O_2$ $[M + H]^+$, 450.1619; found, 450.1690.

4.10. Computational Studies. *4.10.1. Homology Modeling.* The primary sequence of *h*TRPV1 was retrieved from UniProtKB (accession: Q8NER1), and the transmembrane region (residues 417−712) was used in the homology modeling. As template structures, the cryo-EM structures of *r*TRPV1 bound to RTX (PDB id: 5IRX)[8] and CAPZ (PDB id: 5IS0)[8] were used for the agonist-bound and antagonist-bound models, respectively. The corresponding residues from Asn604 to Ser627 of *h*TRPV1 were not solved in the template structure and identified as being located far from the ligand-binding site; these 24 residues were truncated. Based on the sequence alignment using the Clustal program,[25] the homology model of the *h*TRPV1 monomer was constructed using the "Build Homology Models" protocol of MODELER 9v15[26] implemented in Discovery Studio. The bound ligands were copied during the model building. The 10 models were derived, and the model with the lowest probability density function total energy was chosen for further optimization. The models were further refined by using the "Loop refinement (MODELER)" and "Side-chain refinement" protocols. After building the tetrameric model by aligning the monomer models to the tetrameric template structure, the transmembrane region was predicted by performing the "Add Membrane and Orient Molecule" protocol with the Generalized Born with simple SWitching (GBSW)[27] as an implicit solvent model. The generated tetramer model with the implicit membrane was energy minimized using the CHARMM force field with partial charges of CFF. The GBSW implicit solvent model was used with the dielectric constant set as 2 for the membrane nonpolar region and an implicit solvent dielectric constant set as 80 for the water solvent. Some constraints such as harmonic restraints to the backbone atoms with a force constant of 5 and the SHAKE constraint to the bonds including hydrogen atoms were applied.

4.10.2. MD Simulations. The final models were subjected to MD simulations using GROMACS v.5.1.4[28] with CHARMM36 force fields.[29] The input system with the 1-palmitoyl-2-oleoyl-*sn*-glycero-3-phosphatidylcholine lipid membrane was constructed by using the "Membrane Builder" module in CHARM-GUI.[30] The system was solvated with explicit water molecules and ionized with 0.15 M NaCl. After 10 ns equilibration with the *NVT* ensemble, the production runs with the *NPT* ensemble were carried out for 100 ns. From the final 30 ns simulated trajectories, 300 protein conformations were sampled and clustered using the clustering tool in the VMD plugin to calculate and visualize the clusters of conformations. The clustering was carried out with the residues within 6 Å of the complexed ligand. The number of target clusters was set to 3 and a distance function was set to a rmsd with a cutoff of 1.0 Å as the maximal distance value between two similar frames. After clustering the protein conformations into 11 clusters, the conformations with the lowest total energy were selected from each cluster.

4.10.3. Ensemble Docking. Each of the protein conformation was prepared using the "Protein Preparation Wizard" implemented in Maestro v. 11.4 (Schrodinger, LLC, NY). 3D structures of the ligands were prepared using the "LigPrep" module in Maestro. The generation of ionization states significantly populated in pH 7.4 was performed with Ionizer. The geometries of the generated structures were energy-minimized using optimized potential for liquid simulation (OPLS) 3 force field,[31] while keeping the chirality from the input files throughout the calculations. The ensemble docking studies were performed using the "Virtual screening workflow" protocol, which includes the Glide docking. The grids of all protein conformations were added into the receptor table with the default parameters. The Glide SP docking of the ligand was performed first with a van der Waals radii scaling factor of 0.8 for ligand nonpolar atoms and a partial charge cutoff of 0.15. The 30 poses were generated for each ligand and for each protein conformation, keeping all the good scoring states. The ensemble docking results were then merged to generate a maximum of 30 poses based on the glide Emodel scores. The top five poses of the resulting docked complexes were then refined by energy minimization with the OPLS3 force field.

All of the molecular graphic figures were generated using PyMOL software (http://www.pymol.org). All computational studies were undertaken on an Intel Xeon Octa-Core 2.67 GHz workstation with Linux CentOS release 6.7.

4.10.4. Body Temperature Measurements. The rectal measurement procedure was executed by lifting the tail and inserting a rectal probe thermometer (RET-2, Physitemp Instruments, Clifton, NJ, USA), with minimal restraint achieved by holding the base of the tail. The rectal temperature measurement procedure was executed over 1 min. In this study, we followed the national guidelines for conducting animal experiments. All procedures for animal tests were approved by the Medifron Animal Care and Use Committee (approval number, Medifron 2017-1, IACUC).

■ ASSOCIATED CONTENT

Supporting Information

The Supporting Information is available free of charge at https://pubs.acs.org/doi/10.1021/acs.jmedchem.0c00982.

HPLC purities of the final compounds and the figures of molecular modeling (PDF)

Molecular formula strings and biological data (PDB)

3D representation of Figure 3 (PDB)

Molecular formula strings of the prepared compounds (CSV)

■ AUTHOR INFORMATION

Corresponding Authors

Jeewoo Lee − *Laboratory of Medicinal Chemistry, College of Pharmacy, Seoul National University, Seoul 08826, Republic of Korea;* orcid.org/0000-0002-7832-6719; Phone: 82-2-880-7846; Email: jeewoo@snu.ac.kr; Fax: 82-2-888-0649

Sun Choi − *Laboratory of Molecular Modeling & Drug Design, College of Pharmacy and Graduate School of Pharmaceutical Sciences, Ewha Womans University, Seoul 03760, Republic of Korea;* orcid.org/0000-0002-7669-7954; Phone: 82-2-

3277-4503; Email: sunchoi@ewha.ac.kr; Fax: 82-2-3277-2851

Authors

Shivaji A. Thorat − *Laboratory of Medicinal Chemistry, College of Pharmacy, Seoul National University, Seoul 08826, Republic of Korea*

Yoonji Lee − *Laboratory of Molecular Modeling & Drug Design, College of Pharmacy and Graduate School of Pharmaceutical Sciences, Ewha Womans University, Seoul 03760, Republic of Korea; College of Pharmacy, Chung-Ang University, Seoul 06974, Korea*

Aeran Jung − *Laboratory of Medicinal Chemistry, College of Pharmacy, Seoul National University, Seoul 08826, Republic of Korea*

Jihyae Ann − *Laboratory of Medicinal Chemistry, College of Pharmacy, Seoul National University, Seoul 08826, Republic of Korea*

Songyeon Ahn − *Laboratory of Medicinal Chemistry, College of Pharmacy, Seoul National University, Seoul 08826, Republic of Korea*

Jisoo Baek − *Laboratory of Medicinal Chemistry, College of Pharmacy, Seoul National University, Seoul 08826, Republic of Korea*

Dongxu Zuo − *Laboratory of Medicinal Chemistry, College of Pharmacy, Seoul National University, Seoul 08826, Republic of Korea*

Nayeon Do − *Laboratory of Medicinal Chemistry, College of Pharmacy, Seoul National University, Seoul 08826, Republic of Korea*

Jin Ju Jeong − *Laboratory of Medicinal Chemistry, College of Pharmacy, Seoul National University, Seoul 08826, Republic of Korea*

Peter M. Blumberg − *Laboratory of Cancer Biology and Genetics, Center for Cancer Research, National Cancer Institute, NIH, Bethesda, Maryland 20892-4255, United States*

Timothy E. Esch − *Laboratory of Cancer Biology and Genetics, Center for Cancer Research, National Cancer Institute, NIH, Bethesda, Maryland 20892-4255, United States*

Noe A. Turcios − *Laboratory of Cancer Biology and Genetics, Center for Cancer Research, National Cancer Institute, NIH, Bethesda, Maryland 20892-4255, United States*

Larry V. Pearce − *Laboratory of Cancer Biology and Genetics, Center for Cancer Research, National Cancer Institute, NIH, Bethesda, Maryland 20892-4255, United States*

Hee-Jin Ha − *Medifron DBT, Ansan-si, Gyeonggi-do 15426, Republic of Korea*

Young Dong Yoo − *Medifron DBT, Ansan-si, Gyeonggi-do 15426, Republic of Korea*

Sunhye Hong − *Laboratory of Molecular Modeling & Drug Design, College of Pharmacy and Graduate School of Pharmaceutical Sciences, Ewha Womans University, Seoul 03760, Republic of Korea*

Complete contact information is available at: https://pubs.acs.org/10.1021/acs.jmedchem.0c00982

Author Contributions

[#]S.A.T. and Y.L. contributed equally

Notes

The authors declare no competing financial interest.

■ ACKNOWLEDGMENTS

This work was supported by the Midcareer Researcher Program (NRF-2019R1A2C2006837) funded by the National Research Foundation of Korea (NRF), the Bio & Medical Technology Development Program (NRF-2019M3E5D4065251) and the Medical Research Center (MRC) grant (no. 2018R1A5A2025286) through the National Research Foundation of Korea (NRF). We thank the Korea Institute of Science and Technology Information (KISTI) National Supercomputing Center for providing computing resources (KSC-2019-CRE-0076). This work was also supported in part by the Intramural Program of the Center for Cancer Research, National Cancer Institute, NIH (project Z1A BC 005270).

■ ABBREVIATIONS

TRPV1, transient receptor potential vanilloid 1; cryo-EM, transmission electron cryomicroscopy; *h*TRPV1, human TRPV1; *r*TRPV1, rat TRPV1; SAR, structure activity relationship; RTX, resiniferatoxin; CHO, Chinese hamster ovary; FLIPR, fluorometric imaging plater reader; HEK, human embryonic kidney; BCTC, 4-(3-chloro-2-pyridinyl)-*N*-[4-(1,1-dimethylethyl)phenyl]-1-piperazinecarboxamide; ip, intraperitoneal; MD, molecular dynamics; rmsd, root mean squared deviation

■ REFERENCES

(1) Szallasi, A.; Blumberg, P. M. Vanilloid (capsaicin) Receptors and Mechanisms. *Pharmacol. Rev.* **1999**, *51*, 159−212.

(2) Aghazadeh Tabrizi, M.; Baraldi, P. G.; Baraldi, S.; Gessi, S.; Merighi, S.; Borea, P. A. Medicinal Chemistry, Pharmacology, and Clinical Implications of TRPV1 Receptor Antagonists. *Med. Res. Rev.* **2017**, *37*, 936−983.

(3) Caterina, M. J.; Schumacher, M. A.; Tominaga, M.; Rosen, T. A.; Levine, J. D.; Julius, D. The Capsaicin Receptor: a Heat-activated Ion Channel in the Pain Pathway. *Nature* **1997**, *389*, 816−824.

(4) Tominaga, M.; Caterina, M. J.; Malmberg, A. B.; Rosen, T. A.; Gilbert, H.; Skinner, K.; Raumann, B. E.; Basbaum, A. I.; Julius, D. The Cloned Capsaicin Receptor Integrates Multiple Pain-producing Stimuli. *Neuron* **1998**, *21*, 531−543.

(5) Morales-Lázaro, S. L.; Simon, S. A.; Rosenbaum, T. Inhibition of TRPV1 Channels by a Naturally Occurring Omega-9 Fatty Acid Reduces Pain and Itch. *J. Physiol.* **2013**, *591*, 3109−3121.

(6) Szolcsányi, J.; Sándor, Z. Multisteric TRPV1 nocisensor: A Target for Analgesics. *Trends Pharmacol. Sci.* **2012**, *33*, 646−655.

(7) Liao, M.; Cao, E.; Julius, D.; Cheng, Y. Structure of the TRPV1 Ion Channel Determined by Electron Cryo-microscopy. *Nature* **2013**, *504*, 107−112.

(8) Gao, Y.; Cao, E.; Julius, D.; Cheng, Y. TRPV1 Structures in Nanodiscs Reveal Mechanisms of Ligand and Lipid Action. *Nature* **2016**, *534*, 347−351.

(9) Anand, P.; Bley, K. Topical Capsaicin for Pain Management: Therapeutic Potential and Mechanism of Action of the New High-concentration Capsaicin 8% Patch. *Br. J. Anaesth.* **2011**, *107*, 490−502.

(10) Garami, A.; Shimansky, Y. P.; Pakai, E.; Oliveira, D. L.; Gavva, N. R.; Romanovsky, A. A. Contributions of Different Modes of TRPV1 Activation to TRPV1 Antagonist-induced Hyperthermia. *J. Neurosci.* **2010**, *30*, 1435−1440.

(11) Reilly, R. M.; McDonald, H. A.; Puttfarcken, P. S.; Joshi, S. K.; Lewis, L.; Pai, M.; Franklin, P. H.; Segreti, J. A.; Neelands, T. R.; Han, P.; Chen, J.; Mantyh, P. W.; Ghilardi, J. R.; Turner, T. M.; Voight, E. A.; Daanen, J. F.; Schmidt, R. G.; Gomtsyan, A.; Kort, M. E.; Faltynek, C. R.; Kym, P. R. Pharmacology of Modality-specific Transient Receptor Potential Vanilloid-1 Antagonists That Do Not Alter Body Temperature. *J. Pharmacol. Exp. Ther.* **2012**, *342*, 416−428.

(12) Garami, A.; Pakai, E.; McDonald, H. A.; Reilly, R. M.; Gomtsyan, A.; Corrigan, J. J.; Pinter, E.; Zhu, D. X. D.; Lehto, S. G.; Gavva, N. R.;

Kym, P. R.; Romanovsky, A. A. TRPV1 Antagonists That Cause Hypothermia, Instead of Hyperthermia, in Rodents: Compounds' Pharmacological Profiles, In Vivo Targets, Thermoeffectors Recruited and Implications for Drug Development. *Acta Physiol.* **2018**, *223*, No. e13038.
(13) Garami, A.; Shimansky, Y. P.; Rumbus, Z.; Vizin, R. C. L.; Farkas, N.; Hegyi, J.; Szakacs, Z.; Solymar, M.; Csenkey, A.; Chiche, D. A.; Kapil, R.; Kyle, D. J.; Van Horn, W. D.; Hegyi, P.; Romanovsky, A. A. Hyperthermia Induced by Transient Receptor Potential Vanilloid-1 (TRPV1) Antagonists in Human Clinical Trials: Insights from Mathematical Modeling and Meta-analysis. *Pharmacol. Ther.* **2020**, *208*, 107474.
(14) Ann, J.; Kim, H. S.; Thorat, S. A.; Kim, H.; Ha, H.-J.; Choi, K.; Kim, Y.-H.; Kim, M.; Hwang, S. W.; Pearce, L. V.; Esch, T. E.; Turcios, N. A.; Blumberg, P. M.; Lee, J. Discovery of Nonpungent Transient Receptor Potential Vanilloid 1 (TRPV1) Agonist as Strong Topical Analgesic. *J. Med. Chem.* **2020**, *63*, 418−424.
(15) Kim, M. S.; Ryu, H.; Kang, D. W.; Cho, S.-H.; Seo, S.; Park, Y. S.; Kim, M.-Y.; Kwak, E. J.; Kim, Y. S.; Bhondwe, R. S.; Kim, H. S.; Park, S.-g.; Son, K.; Choi, S.; DeAndrea-Lazarus, I. A.; Pearce, L. V.; Blumberg, P. M.; Frank, R.; Bahrenberg, G.; Stockhausen, H.; Kögel, B. Y.; Schiene, K.; Christoph, T.; Lee, J. 2-(3-Fluoro-4-methylsulfonylaminophenyl)propanamides as Potent Transient Receptor Potential Vanilloid 1 (TRPV1) Antagonists: Structure-Activity Relationships of 2-Amino Derivatives in the N-(6-Trifluoromethylpyridin-3-ylmethyl) C-region. *J. Med. Chem.* **2012**, *55*, 8392−8408.
(16) Ahn, S.; Kim, Y. S.; Kim, M. S.; Ann, J.; Ha, H.; Yoo, Y. D.; Kim, Y. H.; Blumberg, P. M.; Frank-Foltyn, R.; Bahrenberg, G.; Stockhausen, H.; Christoph, T.; Lee, J. Discovery of Indane Propanamides as Potent and Selective TRPV1 Antagonists. *Bioorg. Med. Chem. Lett.* **2020**, *30*, 126838.
(17) Boekelheide, V.; Lehn, W. L. The Rearrangement of Substituted Pyridine N-oxides with Acetic Anhydride. *J. Org. Chem.* **1961**, *26*, 428−430.
(18) Pearce, L. V.; Ann, J.; Jung, A.; Thorat, S. A.; Herold, B. K. A.; Habtemichael, A. D.; Blumberg, P. M.; Lee, J. Novel Radiolabeled Vanilloid with Enhanced Specificity for Human Transient Receptor Potential Vanilloid 1 (TRPV1). *J. Med. Chem.* **2017**, *60*, 8246−8252.
(19) Lee, S.; Kim, C.; Ann, J.; Thorat, S. A.; Kim, E.; Park, J.; Choi, S.; Blumberg, P. M.; Frank-Foltyn, R.; Bahrenberg, G.; Stockhausen, H.; Christoph, T.; Lee, J. Pyrazole C-region Analogues of 2-(3-Fluoro-4-methylsulfonylaminophenyl)propanamides as Potent TRPV1 Antagonists. *Bioorg. Med. Chem. Lett.* **2017**, *27*, 4383−4388.
(20) (a) Laskowski, R. A.; Rullmannn, J. A.; MacArthur, M. W.; Kaptein, R.; Thornton, J. M. AQUA and PROCHECK-NMR: Programs for Checking the Quality of Protein Structures Solved by NMR. *J. Biomol. NMR* **1996**, *8*, 477−486. (b) Morris, A. L.; MacArthur, M. W.; Hutchinson, E. G.; Thornton, J. M. Stereochemical Quality of Protein Structure Coordinates. *Proteins* **1992**, *12*, 345−364.
(21) Colovos, C.; Yeates, T. O. Verification of Protein Structures: Patterns of Nonbonded Atomic Interactions. *Protein Sci.* **1993**, *2*, 1511−1519.
(22) Lee, Y.; Lazim, R.; Macalino, S. J. Y.; Choi, S. Importance of Protein Dynamics in the Structure-based Drug Discovery of Class A G Protein-coupled Receptors (GPCRs). *Curr. Opin. Struct. Biol.* **2019**, *55*, 147−153.
(23) Gaulton, A.; Hersey, A.; Nowotka, M.; Bento, A. P.; Chambers, J.; Mendez, D.; Mutowo, P.; Atkinson, F.; Bellis, L. J.; Cibrián-Uhalte, E.; Davies, M.; Dedman, N.; Karlsson, A.; Magariños, M. P.; Overington, J. P.; Papadatos, G.; Smit, I.; Leach, A. R. The ChEMBL Database in 2017. *Nucleic Acids Res.* **2017**, *45*, D945−D954.
(24) Voigt, J. H.; Bienfait, B.; Wang, S.; Nicklaus, M. C. Comparison of the NCI Open Database with Seven Large Chemical Structural Databases. *J. Chem. Inf. Comput. Sci.* **2001**, *41*, 702−712.
(25) Sievers, F.; Higgins, D. G. Clustal Omega, Accurate Alignment of Very Large Numbers of Sequences. *Methods Mol. Biol.* **2014**, *1079*, 105−116.
(26) Webb, B.; Sali, A. Protein Structure Modeling with MODELLER. *Methods Mol. Biol.* **2017**, *1654*, 39−54.
(27) Arthur, E. J.; Brooks, C. L., 3rd Parallelization and Improvements of the Generalized Born Model with a Simple sWitching Function for Modern Graphics Processors. *J. Comput. Chem.* **2016**, *37*, 927−939.
(28) Pronk, S.; Páll, S.; Schulz, R.; Larsson, P.; Bjelkmar, P.; Apostolov, R.; Shirts, M. R.; Smith, J. C.; Kasson, P. M.; van der Spoel, D.; Hess, B.; Lindahl, E. GROMACS 4.5: a High-throughput and Highly Parallel Open Source Molecular Simulation Toolkit. *Bioinformatics* **2013**, *29*, 845−854.
(29) Vanommeslaeghe, K.; Hatcher, E.; Acharya, C.; Kundu, S.; Zhong, S.; Shim, J.; Darian, E.; Guvench, O.; Lopes, P.; Vorobyov, I.; Mackerell, A. D., Jr. CHARMM General Force Field: A Force Field for Drug-like Molecules Compatible with the CHARMM All-atom Additive Biological Force Fields. *J. Comput. Chem.* **2010**, *31*, 671−690.
(30) (a) Lee, J.; Cheng, X.; Swails, J. M.; Yeom, M. S.; Eastman, P. K.; Lemkul, J. A.; Wei, S.; Buckner, J.; Jeong, J. C.; Qi, Y.; Jo, S.; Pande, V. S.; Case, D. A.; Brooks, C. L., III; MacKerell, A. D., Jr.; Klauda, J. B.; Im, W. CHARMM-GUI Input Generator for NAMD, GROMACS, AMBER, OpenMM, and CHARMM/OpenMM Simulations Using the CHARMM36 Additive Force Field. *J. Chem. Theory Comput.* **2016**, *12*, 405−413. (b) Ghahremanpour, M. M.; Arab, S. S.; Aghazadeh, S. B.; Zhang, J.; van der Spoel, D. MemBuilder: A Web-based Graphical Interface to Build Heterogeneously Mixed Membrane Bilayers for the GROMACS Biomolecular Simulation Program. *Bioinformatics* **2014**, *30*, 439−441.
(31) Harder, E.; Damm, W.; Maple, J.; Wu, C.; Reboul, M.; Xiang, J. Y.; Wang, L.; Lupyan, D.; Dahlgren, M. K.; Knight, J. L.; Kaus, J. W.; Cerutti, D. S.; Krilov, G.; Jorgensen, W. L.; Abel, R.; Friesner, R. A. OPLS3: A Force Field Providing Broad Coverage of Drug-like Small Molecules and Proteins. *J. Chem. Theory Comput.* **2016**, *12*, 281−296.

https://dx.doi.org/10.1021/acs.jmedchem.0c00982
J. Med. Chem. 2021, 64, 370−384